

AD632520

AD

# USAAVLABS TECHNICAL REPORT 65-79

## AN INVESTIGATION OF END PLATES TO REDUCE THE DRAG OF PLANAR WINGS

By

Seán C. Roberts

January 1966

U. S. ARMY AVIATION MATERIEL LABORATORIES  
FORT EUSTIS, VIRGINIA

CONTRACT DA 44-177-AMC-892(T)

MISSISSIPPI STATE UNIVERSITY  
STATE COLLEGE, MISSISSIPPI

Distribution of this document is unlimited.



CLEARINGHOUSE FOR FEDERAL SCIENTIFIC AND TECHNICAL INFORMATION			
Hardcopy	Microfiche		
\$ 3.00	\$ .75	67 pp	78
ARCHIVE COPY			

Code 1

### Disclaimers

The findings in this report are not to be construed as an official Department of the Army position unless so designated by other authorized documents.

When Government drawings, specifications, or other data are used for any purpose other than in connection with a definitely related Government procurement operation, the United States Government thereby incurs no responsibility nor any obligation whatsoever; and the fact that the Government may have formulated, furnished, or in any way supplied the said drawings, specifications, or other data is not to be regarded by implication or otherwise as in any manner licensing the holder or any other person or corporation, or conveying any rights or permission, to manufacture, use, or sell any patented invention that may in any way be related thereto.

### Disposition Instructions

Destroy this report when it is no longer needed. Do not return it to the originator.



DEPARTMENT OF THE ARMY  
U. S. ARMY AVIATION MATERIEL LABORATORIES  
FORT EUSTIS, VIRGINIA 23604

This report has been reviewed by the U. S. Army Aviation Materiel Laboratories and is considered to be technically sound. The report is published for the exchange of information and the stimulation of ideas.

Task 1P121401A14203  
Contract DA 44-177-AMC-892(T)  
USAAVLABS Technical Report 65-79  
January 1966

AN INVESTIGATION OF END PLATES  
TO REDUCE THE DRAG OF PLANAR WINGS

Aerophysics Research Report No. 58

By

Seán C. Roberts

Prepared by  
The Aerophysics Department  
Mississippi State University  
State College, Mississippi

for  
U. S. ARMY AVIATION MATERIEL LABORATORIES  
FORT EUSTIS, VIRGINIA

Distribution of this  
document is unlimited.

### ABSTRACT

An analytical and experimental study has been performed to determine the optimum design of end plates which have minimum parasite drag and maximum effect on induced drag. Experiments were performed in a smoke tunnel and at full-scale Reynolds numbers on a modified PA-18 Super Cub aircraft. Flat end plates were found to be relatively ineffectual as a means of reducing the induced drag of aircraft, and the undesirable effect of large flat plates on the directional stability of an aircraft was an important effect to be considered. Cambered wing tip plates are worthy of further consideration, since a 15 percent decrease of induced drag with a 12 percent increase of L/D ratio was obtained from the configurations tested.

CONTENTS

	<u>Page</u>
ABSTRACT -----	iii
LIST OF ILLUSTRATIONS -----	vii
LIST OF SYMBOLS -----	ix
INTRODUCTION -----	1
THEORETICAL ANALYSIS -----	3
SMOKE TUNNEL STUDIES -----	6
FLIGHT TESTS -----	9
CONCLUDING REMARKS AND RECOMMENDATIONS FOR FUTURE RESEARCH ----	17
REFERENCES -----	47
DISTRIBUTION -----	48
APPENDICES	
I. Procedure for the Mathematical Determination of Isobars about an Arbitrary Airfoil Section -----	49
II. Determination of the Effective Aspect Ratio and Induced Drag Coefficient from an Arbitrary Spanwise Wing Loading -----	53

**BLANK PAGE**

LIST OF ILLUSTRATIONS

<u>Figure</u>		<u>Page</u>
1	Plot of the Isobars About the PA-18 Airfoil Section --	19
2	The Smoke Tunnel Used in the Flow Visualization Experiments -----	20
3	Model Wing With Tip Plates -----	21
4	Smoke Photographs of Wing Tip Vortices -----	22
5	Typical Photographs of the Smoke Taken Axially From Behind the Vortices -----	23
6	Tangential Velocity Profiles of the Wing Tip Vortices-	24
7	PA-18 Aircraft Used in the Flight Tests -----	25
8	Installation of the Photographic Manometer in the Test Aircraft -----	26
9	Flat Plate Tip Plates Tested on PA-18 Aircraft -----	27
10	Views of the Cambered Tip Plates Attached to the Aircraft -----	28
11	Tuft Pictures of the Flow at the Intersection of the Cambered Tip Plate and the Wing With and Without the Fillet -----	29
12	Tuft Pictures of the Flow About Various Tip Plates ---	30
13	Smoke Rake Installation on PA-18 Aircraft -----	31
14a	Typical Flow Patterns Behind the Wing Tips With No Tip Plates -----	32
14b	Flow Patterns Behind the Wing Tips With the Cambered Tip Plates -----	33
15	Typical Series of Dust Bomb Photographs -----	34
16	Effect of End Plates on the Wing Tip Vortices -----	35
17	Typical Chordwise Pressure Distributions -----	36

<u>Figure</u>	<u>Page</u>
18	Typical Spanwise Loading Curves for Various Aircraft Airspeeds ----- 37
19	Typical Rate of Sink Results for the PA-18 Aircraft With Various Tip Configurations ----- 38
20a	Drag Polars of the PA-18 Aircraft With Various Tip Configurations With No Flaps ----- 39
20b	Drag Polars of the PA-18 Aircraft With Various Tip Configurations With Full Flaps ----- 40
21a	Lift to Drag Ratios of the PA-18 Aircraft With Various Tip Configurations as a Function of Lift Coefficient With No Flaps ----- 41
21b	Lift to Drag Ratios of the PA-18 Aircraft With Various Tip Configurations as a Function of Lift Coefficient With Full Flaps ----- 41
22a	Plots of $C_D$ vs $C_L^2$ for Various Wing Tip Configurations With No Flaps ----- 42
22b	Plots of $C_D$ vs $C_L^2$ for Various Wing Tip Configurations With Full Flaps ----- 43
23	Effect of Cambered End Plates on Induced Drag Coefficient ----- 44
24	Plot of Plate Area Against Induced Drag Coefficient, $C_L = 1.0$ ----- 45
25	Plot of Plate Area Against Effective Aspect Ratio --- 46

LIST OF SYMBOLS

$\theta$	angle between $\kappa$ and the $x$ axis
$\phi$	angle between spanwise direction and point on the lift distribution curve
$\delta$	angle between $x$ axis and a line from the origin to the center of the circle to be transformed
$\beta$	angle between $x$ axis and a line from the rear stagnation point to the center of the circle to be transformed
$\alpha$	angle defined as $\alpha = \arcsin C_L / 2\pi(1+\epsilon) - \beta$
$R$	aspect ratio
$x, y, z$	cartesian coordinates
$c$	chord
$K$	circulation
$V$	connected aircraft rate of sink
$k$	constant
$A_n$	constants of Fourier series, $n = 1, 2, 3, \dots$
$\rho$	density
$r$	distance from the origin of the $z$ coordinate system to a point in the $z$ plane
$m$	distance from the origin to the center of the circle to be transformed
$C_1$	distance from the origin to the rear stagnation point of a circle to be transformed into an airfoil
$w$	downwash velocity
$q_\infty$	dynamic head = $\frac{1}{2} \rho U_\infty^2$
$Re$	effective aspect ratio
$M$	Fourier series representing spanwise loading
$U_\infty$	freestream velocity

$D_i$	induced drag
$C_{D_i}$	induced drag coefficient
$z, \xi, \eta$	Joukowski transformation coordinates
$C_L$	lift coefficient
$q$	local velocity in the $z$ plane
$e$	natural logarithm base
$C_{D_0}$	parasite drag coefficient
$P_{re}$	power required
$R$	radius
$a$	radius of circle to be transformed
$\frac{dh}{dt}$	rate of sink, uncorrected for temperature
$C_f$	skin friction coefficient
$D_f$	skin friction drag
$T_s$	standard temperature, degrees absolute
$C_p$	static pressure coefficient
$\psi$	stream function in potential theory
$V_t$	tangential velocity
$T_T$	test temperature, degrees absolute
$T$	thickness of airfoil
$\epsilon$	thickness parameter, $\epsilon = 0.77 \frac{T}{C}$
$S_P$	tip plate area
$D$	total aircraft drag
$C_D$	total drag coefficient
$\bar{V}$	$\bar{V} = a U_\infty (1 + \epsilon^2) / C_1 (1 + \epsilon)$
$u$	velocity in the $x$ direction

**V** velocity in the **y** direction

**w** weight

**S<sub>w</sub>** wing area

**L** wing lift

**S** wing semispan

**BLANK PAGE**

## INTRODUCTION

The drag of an aircraft can generally be divided into two categories: that which is due to viscous effects and that which is due to lift. The viscous drag including the interference drag and pressure drag is termed the parasite drag. The drag due to the lift is called the induced drag. Parasite drag has been the primary concern of aerodynamicists since the inception of high-speed vehicles. At the present time in subsonic incompressible flow, vehicles can be designed with a parasite drag approaching the minimum, which can be taken as the drag of the equivalent flat plate in turbulent flow. However, the drag induced by the three-dimensional lifting surfaces of vehicles is relatively unexplored, and it still remains a stumbling block in the field of incompressible viscous drag.

Induced drag investigations have been relatively few until recently, due to the fact that the maximum lift coefficients which could be attained by conventional wings were relatively small. However, with the advent of high-lift boundary layer control systems which are capable of giving local lift coefficients of the order of 6.0, induced drag becomes a major problem. Although there are a few aircraft which can attain lift coefficients greater than 5.0, it is difficult to fly these aircraft in turbulent air at high-lift coefficients due to the fact that the speed of the aircraft is unstable because it is on the backside of the drag curve; i.e.,  $\frac{d(DRAG)}{d(VEL)}$  is negative. There are two approaches to the problem: one, to develop an automatic device that can handle the large corrections necessary for high-lift flight in turbulent air; the other, to cure the cause of the problem which is the build-up in induced drag. The former solution would perhaps suffer from a lack of response in engine power or elevator effectiveness and would be, at best, only a temporary solution to the problem.

The induced drag of a lifting surface is closely linked with the tip vortices, the strength of which is a function of wing lift coefficient and aspect ratio. Wing tip vortices, besides having a large effect on high-lift aircraft in the low-speed regime, are important in areas of downwash velocities, tunnel wall interference, influence of lead aircraft on chase aircraft, aerodynamic loads on tailplanes, and aircraft separation in high-density traffic areas. In all of the areas mentioned above, the primary motive of investigation is to reduce the wing tip vortex strength and thereby reduce the induced drag. However, there are applications, as in agricultural aircraft, where wing tip vortices are used to spread the ejected material evenly onto the ground and to increase the effective swath width of the distribution systems (references 10 and 12).

It is known that effective end plating completely eliminates the tip vortices and that the induced drag is zero, which is the same solution as a wing with infinite span. If infinite end plates eliminate the tip vortices, then smaller end plates will reduce the tip vortex strength and hence the induced drag by a proportional amount. However, the presence of

the end plates increases the wetted area of the lifting system, and the parasite drag is increased. The ratio of the reduction in induced drag and the increase in parasite drag will determine the feasibility of end plating to reduce induced drag.

This report deals with a theoretical and experimental study of optimum design end plates which have minimum parasite drag and effect a maximum reduction in induced drag. Experiments were performed in a smoke tunnel and at full-scale Reynolds numbers on a modified PA-18 Super Cub aircraft.

**BLANK PAGE**

## THEORETICAL ANALYSIS

### OPTIMUM DESIGN OF END PLATES FOR FINITE PLANE WINGS

In the design of end plates to reduce the induced drag of three-dimensional wings, the skin friction drag caused by the plates must be considered. For the sake of simplicity, the interference drag between the plate and the wing shall be neglected, although in later evaluations it could easily be considered. The effect of end plates on the stability derivatives are also neglected, even though they could be very important if increases in fin area were required to maintain adequate directional stability. This effect, however, could best be judged for individual aircraft rather than for the general case.

Induced drag =  $C_{Di} q_{\infty} S_w = D_i$ , (1)  
and assuming an average value for skin friction on the plate, the drag of two plates, one on each tip, is then  $D_f$ .

$$D_f = 4 C_f q_{\infty} S_p, \quad (2)$$

where  $C_f$  is the average value of skin friction assumed for the analysis. Let reduction in induced drag due to end plates be  $n D_i$ , so that ratio of induced drag reduction to plate drag is then

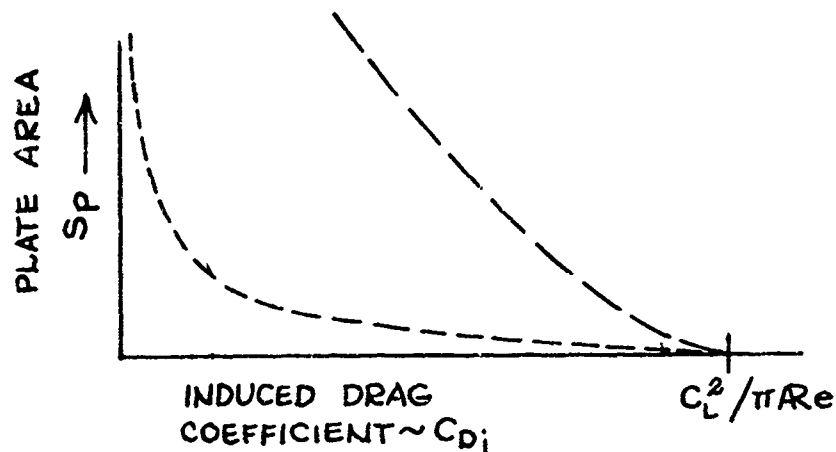
$$\frac{n D_i}{D_f} = \frac{n C_{Di} q_{\infty} S_w}{4 C_f q_{\infty} S_p}. \quad (3)$$

If it is assumed that  $C_{Di}$  can be expressed in the form  $\frac{C_L^2}{\pi A Re}$ , then equation (3) can be written

$$\frac{n D_i}{D_f} = \frac{n}{4 \pi C_f} \frac{C_L^2 S_w}{A Re S_p}. \quad (4)$$

If a reduction in drag is to be realized, this ratio must be greater than unity. However, several functions must first be found quantitatively before further analysis is possible. If it is assumed that the end plates will take the shape of an isobar around the airfoil, then the area of the plate is a function of the chosen value of pressure coefficient. The variations of the plate area with the isobar depend upon the airfoil section and the lift coefficient. It is then necessary to determine the amount by which the induced drag is reduced by the presence of the plate. Obviously, the maximum reduction could be the total reduced drag

$$C_L^2 / \pi A Re.$$



The shape of the curve of plate area against induced drag is very important, as this will determine primarily whether end plates will be used for induced drag reduction. For example, the upper curve in the diagram would be unfavourable toward end plates, whereas the lower curve shows that, for relatively small plate areas, considerable reduction in induced drag could be attained.

#### DETERMINATION OF THE ISOBARS FOR THE FLAT PLATE EXPERIMENTS

When end plates are designed, generally there is relatively little thought given to the shape of the end plates, except perhaps that it be something that resembles the airfoil section with a certain size flange. Hoerner suggests that any end plate exceeding the wing chord does not contribute much to the situation, that the effect on induced drag is indifferent to location and positioning of the plates, and that the height of the plate is the all-important variable. Contrary to the above hypothesis, it has been assumed in this report that the end plates take the shape of the isobars on the airfoil so that all pressures lower than the value chosen will be contained by the end plate. This assumption, of course, makes the area, shape, and position of the end plate on the wing tip very important. The technique of using the isobars as a guide to define the shape of a tip would, a priori, seem to be the minimum size to contain certain pressures and, therefore, would have minimum parasite drag.

The mathematical determination of the isobars is a simple application of basic airfoil theory utilizing a Joukowski transformation and the flow around a cylinder with circulation. A circle is chosen that will produce a Joukowski airfoil that is the closest approximation to the experimental airfoil. Variations of the camber and thickness can be used to produce relatively close approximations. The circulation is then calculated for several aerodynamic conditions, and the streamlines are calculated and transformed. The local velocities along the streamlines are calculated and plotted. When equal velocity points are connected, the resulting curve is a constant pressure line of the desired pressure coefficient. The procedure is described in detail in Appendix I, and the results for the PA-18

are shown in Figure 1.

#### CAMBERED END PLATES

Perhaps a look at nature might help in the design of end plates; for example, the black buzzard has a problem very similar to certain aircraft, in that he is bothered by induced drag. His wing loading is relatively high because he must be strong; but since he sails close to the ground where the thermals are narrow, he must be able to execute a small-radius turn, which means slow-speed flying. When flying slowly to stay in thermals, very small wings suffer from Reynolds number problems, in that laminar separation is very prevalent; therefore, to overcome the problem, it is necessary for the buzzard to have a large chord airfoil. Because this predatory bird operates from forests and swampy regions where obstacles are numerous, it is necessary for his wing span to be small; otherwise, takeoff and landing would constitute a hazardous condition. Since the buzzard must travel considerable distances in search of food, he must be able to soar in the small thermals close to the ground. Unfortunately, high aspect ratios are impossible due to entanglement possibilities in takeoff; therefore, he must have some means by which he can artificially increase his effective aspect ratio. This seems to be accomplished by means of his tip feathers (references 5 and 8). The seven tip feathers are bent upward, with the leading edge feather nearly vertical and the angle decreasing so the last trailing edge feather is bent slightly downward. Each feather is an airfoil in its own right, with the cambered side facing inward so that when airloads are applied to them, they bend upward in the previously described fashion. The difference in bending could be due to difference in rigidity. These feathers at the tip, each with an effective aspect ratio of about 14, give circulation in such a manner as to directly oppose the wing tip vortex which would normally occur. In this manner, the effective aspect ratio of the buzzard can be increased from about 6 to approximately 14 by estimating observed sinking speeds (reference 9).

From these observations on buzzards, it seems probable that controllable cambered wing tips could be made to increase the effective aspect ratio of existing aircraft in certain flight conditions. As a preliminary experiment, perhaps a single fixed cambered end plate the same size as the flat plates designed in the previous section could be used to determine the effect on induced drag. Alternatively, if the induced spanwise flow from these primary wing tip feathers of the buzzard has such a tremendous effect on aspect ratio, it seems probable that a flat sheet of air from a chordwise slot near the tip, ejecting air in a spanwise direction, would be equally effective in reducing the effect of wing tip vortices by moving them away from the tip, thereby decreasing the induced drag.

## SMOKE TUNNEL STUDIES

As a preliminary investigation, prior to the full-scale flight experiments, it was thought that smoke tunnel studies on a semispan wing with and without wing tip plates would give a qualitative insight into the flow about tip plates.

### DESCRIPTION OF THE SMOKE TUNNEL, MODEL AND EXPERIMENTAL APPARATUS

The smoke tunnel used in these tests (Figure 2) has a test section 2 feet square with a large 16 to 1 contraction ratio inlet section with numerous screens which give smooth flow up to test section velocities of 12 feet per second. A rheostat-controlled electric motor on a constant voltage power supply unit provided the power necessary for the fixed-pitch fan, which operated quite well within the range of velocities of the tunnel of 4 feet per second to 12 feet per second. The exhaust from the smoke tunnel was directed out of the room via a window to prevent contamination of the building with smoke fumes. The test section was enclosed by a dark room in which everything was painted black to eliminate reflections when smoke pictures were being taken through the Plexiglas\* windows of the tunnel. For visual observation, two polarized light sources illuminated a plane of the tunnel through the ceiling. These light sources could be moved laterally in the tunnel. A high-intensity strobe flash of 1/1000 second was used for photographic purposes.

The smoke generator consisted primarily of vaporizing oil by means of heating elements wound around a wick trailing in oil. The vapor was pushed, by means of compressed air, through two particle traps of large volumes, and then into a smoke rake located near the screens at the entrance of the contraction section. The supply of compressed air had to be adjusted so the exit velocity of the smoke at the rake was the same as the local velocity to prevent backup of the smoke filaments. The smoke rake could be moved up or down in the test section by means of a screw mechanism driven by an electric motor which was operated from the control room.

The wing model was a semispan wing with the same airfoil section as that used in the PA-18 aircraft on which the flight studies would be performed. The chord was 4 inches and the semispan was 12 inches. The wing was fixed to the wall of the smoke tunnel in such a manner that the airfoil angle of attack could be varied. The end plates, which were fabricated from 1/8-inch Plexiglas, were cut in the shape of isobars that were calculated by theoretical methods described in the preceding section and in Appendix I.

The cameras which were used to record the smoke patterns were 35-millimeter Praktina cameras with 50-millimeter lenses. One was situated

\* Reg. T. M. Rohm & Haas Company

in the control room so that pictures could be taken spanwise into the tip, and the other one was placed in the smoke tunnel diffuser section looking upstream so that photographs could be taken perpendicular to the plane of the wing tip vortex. To ensure that only a particular section behind the tip would be photographed at one time, a plane of polarized light, which could be moved to various positions aft of the wing trailing edge, was used so that only those sections of the smoke filaments which were illuminated would be photographed.

### SMOKE TUNNEL EXPERIMENTS

With the conventional wing in the test section, a series of photographs were taken at distances of 3, 9, 15, and 21 inches behind the wing. The angle of attack of the wing was set at three positions, and the airspeed was varied three times for each angle of attack, giving a series of nine photographs at each position behind the wing. The positions of the smoke streams were stationary relative to the wing throughout the series of shots. The above procedure was repeated for each end plate configuration. Photographs taken from the end of the wing were found to be too unstable to permit comparison between various configurations, and the procedure was abandoned after a few trial runs. Typical photographs taken from behind the wing tip vortex are shown in Figure 5. These photographs showed the streamlines as a series of dots and short streaks, because the only part of the streamline that was illuminated was a 2-inch length where the light cut it. By locating the center of the vortex from the photographs, measuring the distance from the vortex center to a streamline, and measuring the length of the streamline which appeared as a portion of an arc, a tangential velocity profile of each vortex was obtained and plotted (Figure 6). This was possible because the illuminated length of the streamline was known to be 2 inches and the photographed length of the streamline, viewed from an axial direction, was a measure of the amount of rotation in a 2-inch distance. These velocity profiles gave a method of comparing flow pictures of the wing tip vortices with and without end plates.

### DISCUSSION OF RESULTS OF THE SMOKE TUNNEL EXPERIMENTS

The equation of the tangential velocity of a vortex as a function of radius measured from the vortex center is  $V_t = \frac{k}{R}$ . The results of the velocity plots (Figure 6) showed that the tangential velocity was inversely proportional to the radius; however, there was no continuity between the photographs. An individual photograph gave about eight points that formed a good curve of the desired form, but points from different photographs of the same conditions did not necessarily fall on the same curve. Some small degree of similarity existed between photographs taken at the same speed, the same angle of attack, or the same position; but the accuracy and repeatability were poor.

The primary reason for the poor repeatability of the results was a certain instability of the flow in the smoke tunnel caused by back-pressure when the external wind was of the same order of magnitude as the flow through the window from the tunnel fan. The obvious way to overcome this problem would be to accelerate the flow leaving the fan by means of a contraction section which would eject the tunnel air through the window at a much higher velocity than the normal wind velocity. This modification is currently being performed. Other sources of error are possible swirl in the tunnel flow, secondary flow due to having a rectangular test section, variations in smoke density, and the smoke filament thickness causing inaccuracies in measuring the length of the smoke filaments at such small angles to the axial flow.

A plot of the observed tangential velocity against radius for each of the four tip configurations tested (Figure 6) showed that the addition of the plates to the tips of the airfoil, especially plate No. 3, seems to decrease the maximum velocities in the vortex and change the velocity distribution so that the vortex is considerably larger in diameter with approximately the same average velocity but has lower peak velocities. The addition of these plates would appear to be what is required, because with lower peak velocities the efficiency of the system should be increased for a certain value of circulation.

The smoke tunnel tests showed that tangential velocity curves could be plotted from photographs obtained from behind the vortex, as mentioned above, if the flow in the tunnel was axial and steady and if the smoke filaments were small and of consistent density. The addition of the end plates seemed to even out the velocity distribution in the tip vortices.

## FLIGHT TESTS

The smoke tunnel studies showed that end plates apparently did not have much effect on the flow pattern about the wing tip, although quantitative measurements would perhaps show significant differences. Due to the fact that the available wind tunnel was rather small, it was decided to perform some simple flight experiments on a PA-18 high-wing aircraft to determine the effect of end plates on induced drag. Flight experiments would eliminate wall effects that would naturally occur in wind tunnel tests; also, it was thought that Reynolds number effects on wing tip vortices would be appreciable with the result that full-scale flight experiments would be preferable.

## DESCRIPTION OF THE PA-18 AIRCRAFT

The Piper PA-18 Super Cub aircraft is a two-place aircraft that is powered by a 135-horsepower Lycoming engine (Figure 7). Due to the fact that large end plates would be added to the wing tips, thereby causing considerable stress concentrations, an original set of wings were rebuilt so that they could withstand load concentrations of 50 pounds at the wing tips. The wing tips were square with the end rib being sufficiently strong so that the various tip shapes could be attached by means of wood screws. The aircraft weighed 1440 pounds with full tanks and no pilot. The wing span is 33.2 feet, the chord 5.25 feet, the aspect ratio 6.33, and the wing area 174.2 square feet. Five rows of pressure taps were installed on the left wing, each row having 20 pressure taps. The pressure belts were fed to a multichannel photographic manometer capable of simultaneously recording 52 separate "U" tubes. Unfortunately, it was never possible to measure all the rows of pressure taps simultaneously, so it required two flights at the same flight conditions to obtain a spanwise loading distribution; however, this was not a serious limitation on the flight testing procedure, although it was preferable to complete a set of chordwise pressure distributions in one morning to prevent excessive temperature changes.

## END PLATES

The shape of the end plates was calculated according to the isobar method described previously and outlined in Appendix I. Three values of  $C_p$  were chosen, and three sets of end plates were fabricated from  $\frac{1}{2}$ -inch plywood. These plates were attached to the end rib, and they were sufficiently stiff so as not to require any additional braces. The maximum size of the tip plates was limited by the decrease in directional stability with an increase in tip plate size. A preliminary theoretical stability analysis was performed and the maximum size of the tip plates determined without adding to the fin area. Nevertheless, to be sure of the safety aspect, the plates were added in increasing increments and the

directional stability was checked prior to proceeding to the next larger size plates. When the large tip plates were added to the aircraft, all flights were restricted to zero cross-wind conditions on the main 5000-foot runway. The three plate areas tested were 1.43 ft<sup>2</sup>, 6.17 ft<sup>2</sup>, and 11.14 ft<sup>2</sup> (Figure 9).

The cambered plates had the same planform as the medium sized plates, and the airfoil section chosen was that used in the wing of the PA-28. The cambered plates were fabricated from plywood frames and balsa wood contours covered with fabric. The cambered plates were attached to the wing tip with the cambered surface facing inboard as shown in Figure 10. One of the cambered tip plates had two rows of flush-mounted pressure taps fitted so that pressure distributions around the tip could be obtained. Due to flow separation occurring on the inside of the cambered plate at the junction of the wing, a fillet was fabricated to eliminate this interference drag at relatively high angles of attack (see Figure 11 for tuft pictures of the intersection with and without the fillet).

#### POWERED FLIGHT TESTS

Prior to quantitative flight experiments, the airspeed and altimeter instruments in the aircraft were replaced by calibrated sensitive helicopter Kollsman airspeed indicators and altimeters. Static position errors were obtained by comparing the aircraft system to that of a trailing static sonde and a Kiel tube total head mounted on the underside of the wing. The aircraft was also weighed and the horizontal center of gravity position located.

#### Flow Visualization

The flow about the wing tips was visualized by means of tufts which were photographed both from a chase plane (Figure 13) and from a remotely controlled camera mounted on top of the wing of the airplane (Figure 11). The development of the vortex downstream of the tip was visualized by the smoke rake method, which is fully described in reference 11. This method consists of burning a standard smoke grenade in a chamber which feeds into six rakes that disperse the smoke filaments in the flow about the wing tip. The smoke patterns can be photographed either from the ground, if the aircraft flies low and the turbulence and wind on the surface are zero, or from a chase plane, if care is taken that the chase plane itself does not interfere with the wing tip vortices of the lead aircraft. Figures 13 and 14 show the smoke rake installation and typical flow pattern behind the wing tips.

Another method of visualizing the vortex flow is to inject finely granulated dust particles from the wing tip into the vortex flow and to photograph the ensuing formation from the ground at regular intervals. This technique is also described in reference 11 and is quite useful to

gauge the physical size of the vortices, the approximate strength and the rate of decay.

The above flow visualization techniques were applied to all wing tip configurations including the original wing tip and the cambered tip plates.

### Pressure Distribution

Chordwise pressure distributions were recorded photographically on the multitube water manometer, two rows at a time, for constant conditions of airspeed, engine r.p.m., and altitude. Efforts were also made to maintain the aircraft weight constant by means of ballast, and the errors due to fuel consumption were found to be very small in comparison to the aircraft weight for short periods of testing. From the pressure data recorded on film, the chordwise pressure distributions for each of the four rows of pressure taps were calculated. The integral of the chordwise pressure distribution gave the local lift coefficient, which was then plotted against the spanwise position of the rows of pressure taps to obtain spanwise lift distributions.

Spanwise loadings were obtained for a number of airspeed readings with the flaps up and with the flaps in the full-down position. Figures 17 and 18 show typical chordwise pressure distributions and spanwise loadings on the PA-18 aircraft with end plates.

### GLIDE TESTS

The powered tests were used primarily to determine the chordwise pressure distributions and the spanwise loadings for various flap and airspeed configurations, and no attempt was made to measure the power required to sustain the aircraft in level flight at various airspeeds. The primary reason for this was to minimize the effects of propeller slipstream on the pressure distribution results by performing all the powered tests at a constant engine r.p.m. This technique precluded any drag measurements from engine data. Drag measurements taken from engine data are generally only relative due to dependence on a specific set of engine curves obtained on an engine test load; this may not be completely representative of the installation in the aircraft. Considerable errors in absolute engine power can be introduced by the rather coarse measurements of engine r.p.m. and manifold pressure; similarly, propeller efficiency determination has appreciable effect on the final thrust results, and accurate determination of propeller efficiency is difficult to obtain.

An alternative method of determining the drag of an airplane, especially when relatively small differences in drag are anticipated with different configurations, is by the use of the gliding technique, which

consists of removing the propeller of the aircraft, sealing the cowling, and installing a tow rope hook and release mechanism. The test aircraft can be towed to altitude by a tow plane, which in this case was a 450-horsepower Stearman aircraft. Towing to 10,000 feet or 15,000 feet generally gave ample testing time to perform accurate flight measurements for the rate of sink for various flight conditions.

### Experimental Techniques

In flight testing where a continual change in pressure occurs as in climbing or descending, care must be taken to ensure that the airspeed indicators used in the test are dynamically balanced, which means that the resistance of both the static and the Pitot sides of the airspeed indicator are equal; otherwise, erroneous readings would result from the change of ambient pressure.

With a calibrated sensitive altimeter, the rate of sink of the aircraft at any airspeed was determined by plotting altitude on a time basis every 100 feet for a range of 1000 feet and taking the slope of the line. The points for any particular airspeed should be on a straight line; any deviation indicates a lack of adequate speed control by the pilot. The result (dh/dt) obtained from the flight test is corrected to standard temperature and pressure conditions to give true sink speeds of the aircraft. With this gliding configuration, the aircraft weight is constant; and when various tip plate configurations were tested, where the weight of the plates was a variable, the aircraft weight was adjusted to the standard test weight by removing quantities of gasoline from the tanks. Total drag coefficients were calculated from the gliding tests by the following formulae.

For relatively shallow gliding angles in still air, the product of the forward velocity and drag approximates the product of aircraft weight and sinking velocity in steady flight conditions; i.e.,

weight x sinking speed = power required = drag x forward velocity  
(reference 6)

$$W \times V = P_{re} = D \times U_{\infty}$$

$$C_D = \frac{1}{\frac{1}{2} \rho U_{\infty}^2 S_w} \left( \frac{WV}{U_{\infty}} \right) = \frac{WV}{\frac{1}{2} \rho U_{\infty}^2 S_w}$$

where  $C_D$  = total aircraft drag coefficient. If  $C_D$  takes the form  $C_{D_0} + C_L^2 / \pi A R e^2$  where  $C_{D_0}$  is the parasite drag coefficient, then a plot of  $C_D$  against  $C_L$  gives values of  $C_{D_0}$  and  $A R e$  (Figure 22).

## FLIGHT TEST RESULTS

The PA-18 aircraft used in the flight tests performed quite adequately as a glider, with lift to drag ratios greater than 9 to 1 with the propeller removed and the cowl sealed. However, the parasite drag of this aircraft is relatively large, i.e.,  $C_{D_0} = .04$  for the flaps-up configuration, so that trying to determine small differences in induced drag was difficult due to the problem of accurately determining small differences between relatively large numbers. Fortunately, the aircraft had ample directional control, allowing plates up to 12 ft<sup>2</sup> to be installed on each wing tip before the directional control was marginal.

The tuft pictures of the various wing tip plates indicated that the effect of the plate is to split the normal single wing tip vortex into a lower and upper pair at the tip; apparently, these two vortices combine into a single vortex quite close to the trailing edge of the wing, as can be clearly seen from the flow visualization pictures of the vortex using the smoke rake (Figure 14b). The preliminary tuft pictures of the flow around the cambered tip plate showed that flow separation occurred at the intersection of the plate and the wing. This condition resulted in an excessive build-up in parasite drag; but the flow separation problem was solved, as can be clearly seen in Figure 11, by the additions of a fillet at the junction of the wing and plate. The smoke rake pictures in Figure 14a show that the wing tip vortex without the tip plate seems to be of small diameter with a clearly defined laminar core and high rotational velocities. The addition of a wing tip plate, for the same aircraft lift coefficient, appears to increase the diameter of the vortex and to reduce the rotational velocities; this indicates that, assuming everything else constant, i.e., constant rotational momentum in both cases, the wing tip plate is more efficient since a larger air mass is traveling at lower velocities.

The flow separation on the inside of the cambered plates was caused by the flow, at relatively large aircraft lift coefficients, coming inboard of the wing tip. Therefore, if a lifting force on the end plates, which is really a side force to the aircraft, is generated, considerable sidewash from the wing tip plate would be noticed. By the use of the dust bomb technique, plots of the horizontal and vertical movements of the vortices with and without end plates at a constant aircraft lift coefficient were obtained. The wing tip plate effected greater lateral movement of the tip vortices with respect to the center line of the flight path (Figure 16). This effect decreases the downwash on the wing due to the vortices and, hence, decreases the induced drag. It is interesting to note that this effect of cambered wing tip plates could possibly be used in the field of aerial application where the effective swath width could be increased by using cambered wing tip plates; also, the induced drag of heavily loaded agricultural aircraft at low airspeeds would be reduced.

The rows of pressure taps in the left wing gave adequate chordwise pressure distributions as seen in Figure 17. Unfortunately, with only

four rows of pressure taps, the accuracy of the spanwise loading curves (Figure 18) is doubtful; however, by the use of a method developed in Appendix II, which utilizes a Fourier synthesis method to describe the spanwise loading curve, values of induced drag and effective aspect ratio were calculated and plotted in Figure 23, where they were compared with those results determined from the glide tests. The results of  $C_{Di}$  as determined from the spanwise loading curves are discussed later in this section.

Due to the inability to accurately determine drag measurements from engine data and also to eliminate the propeller slipstream effects, gliding flight tests were performed where the rate of sink was determined at various airspeeds and wing tip configurations. A typical rate of sink results, which have been corrected for atmospheric temperature, is shown in Figure 19, and it can be clearly seen that the rate of sink generally decreases with an increase in plate area for low airspeeds and high-lift coefficients. At high airspeeds the parasite drag of the large No. 3 plate is obviously high, which increases the aircraft rate of sink. This increase in parasite drag is probably due to flow separation at the intersection of the tip plate and the wing, since it is significant that the No. 2 cambered plate does not suffer from a severe increase in parasite drag.

The curves of total aircraft drag against aircraft lift coefficient for the unflapped case (Figure 20a) indicated that above lift coefficients of 0.7, the total drag of the aircraft is decreased by the addition of the end plates. For the case of the cambered plates, the reduction in total drag is about 10 percent. This means that the reduction in induced drag must be considerably greater than 10 percent to take into consideration the parasite drag of the end plates due to the increase in wetted area and to the interference drag between the wing tip plate and the wing. At lift coefficients of about 0.5, the decrease in induced drag approximately equals the increase in parasite drag, which means that at aircraft airspeeds greater than 80 miles per hour, the effect of the end plate is detrimental to the performance of the aircraft. In the full flap configuration, the percentage decrease in aircraft total drag coefficient is approximately the same as the unflapped airfoil, which means that there is a tremendous build-up in parasite drag to lowering the flaps, i.e., nearly a 100-percent increase in  $C_{D0}$  over the unflapped case, and this increase in parasite drag is compensated for by an equivalent decrease in induced drag, which comes from the airfoil operating at higher lift coefficients.

The effect of the wing tip end plates on the performance of the PA-18 aircraft is clearly shown in Figures 21a and 21b, which are plots of the ratio  $C_L/C_D$  against  $C_L$  for each wing tip configuration. The cambered No. 2 wing tip plates increased the maximum lift to drag ratio at a lift coefficient of 0.8 from 10.1 for the normal wing to 11.25, which represents an increase of 11.4 percent for the unflapped case. It is interesting to note that the small No. 1 plate appears to have a detrimental effect on

the lift to drag ratio over the normal wing configuration. It appears that for the case of the small plate,  $1.48 \text{ ft}^2$ , the decrease in induced drag is small in comparison with the increase in parasite drag. For the full flap case the maximum lift to drag ratio occurs at a lift coefficient of 1.05, and the percentage increase in performance due to the cambered plates is 13.6 percent and 15.5 percent for the large end plate. It is obvious that at large lift coefficients, plate size becomes important; however, the smaller cambered plate, which has about half the plate area as the largest plate, is nearly as effective up to aircraft lift coefficients of 1.4.

The curves of  $C_D$  against  $C_L$ , which were used to determine effective aspect ratios, were reasonably linear up to values of  $C_L = 1.3$  for the unflapped case and  $C_L = 2.2$  for the full-flap case. The values of the aspect ratios determined from these curves are tabulated in Figure 22a and Figure 22b and are plotted against wing tip plate area in Figure 25. It appears that approximately a 10-percent increase in effective aspect ratio was obtained by the use of the cambered No. 2 plate,  $6.17 \text{ ft}^2$ , and about a 7-percent increase with the No. 3 plate,  $11.14 \text{ ft}^2$ , in the unflapped airfoil case. The percentages for the flapped airfoil configuration are slightly smaller than for the unflapped case. The values of effective aspect ratio for the normal wing and the cambered wing tip were taken; and curves of  $C_{D_i}$  against  $C_L$  were obtained as shown by the solid lines in Figure 23. The circles and squares also on this curve are the values of  $C_{D_i}$  obtained from the spanwise loading distributions by the Fourier synthesis method developed in Appendix II. It is reasonably obvious from the random scatter of the results obtained from the spanwise loadings that perhaps the spanwise loadings were not quite accurate; and this is not surprising, considering the fact that these curves were obtained from four points. Four points are adequate when the loading is relatively constant over the span; but when, as in this case, supercirculation can occur at the wing tips due to the effect of the cambered tip plates, four data points are insufficient to obtain an accurate spanwise loading. The solid lines (Figure 23) obtained from the gliding flight tests show that above lift coefficients of 0.7 the average reduction in induced drag is approximately 15 percent for the cambered plates with an area of  $6.17 \text{ ft}^2$ ,

A plot of the induced drag coefficient against wing tip plate area (shown in Figure 24) demonstrates that the flat end plate is relatively ineffective in reducing the induced drag of plane wings. From the four points available, it would appear that, at the very best, a linear function could be assumed for flat plates which makes them unrealistic as a means of increasing the effective aspect ratio. The cambered plate shows much more promise, although the results are for a single configuration. The maximum wing tip plates that could be tolerated on the PA-18 without an increase in vertical fin area are those whose area was  $11.14 \text{ ft}^2$ ; and even then, the maximum crosswind component in landing would be severely reduced.

The plot of the effective aspect ratios against wing tip plate area for the unflapped airfoil indicates that the small tip plates, No. 1, do more harm than good in increasing the effective aspect ratios of an unflapped airfoil, whereas the cambered wing tip plates hold considerable promise as a means of increasing the efficiency of plane three-dimensional wings.

## CONCLUDING REMARKS AND RECOMMENDATIONS FOR FUTURE RESEARCH

The smoke tunnel experiments showed that radial velocity graphs could be plotted from photographs obtained from behind the vortex; however, the results obtained with the present smoke tunnel were unreliable for quantitative measurements, although qualitatively the results indicated that end plates increased the diameter of the wing tip vortex and decreased the tangential velocities.

The PA-18 aircraft performed quite adequately for the full-scale flight tests, and the flow visualization studies, using smoke, verified the observations from the smoke tunnel that tip plates increased the size of the vortices, thereby making the system more efficient. Tuft pictures show considerable flow separation on the inboard side of the flat tip plate at the junction of the plate and the wing with a corresponding increase in drag; however, this separation was successfully eliminated by means of cambered wing tip plates and a fillet at the intersection of the plate and wing tip.

Four rows of pressure taps on one wing were considered insufficient to accurately determine the spanwise loading from which values of induced drag coefficient and effective aspect ratio could be found by means of a Fourier synthesis method developed in Appendix II. The glide tests gave accurate and consistent results which clearly delineated the effect of each wing tip configuration on the aircraft performance. The small flat tip plates, 1.48 ft<sup>2</sup> area, were no improvement over the normal, squared-off tips on this particular PA-18 aircraft. The 6.17 ft<sup>2</sup> flat tip plates gave small increases in performance at lift coefficients greater than 0.5, a 5-percent increase in L/D. The large tip plates of 11.14 ft<sup>2</sup> area gave an increase in L/D of about 7 percent. Considering the tremendous plate area, the increase in parasite drag, and the loss in directional stability, the decrease in induced drag is very small: only about 10- to 15-percent reduction. The cambered wing tip plates seem to be the most promising with respect to increases in effective aspect ratio and L/D ratio for a relatively small plate area; i.e., about 15-percent reduction in induced drag for a plate area of 6.17 ft<sup>2</sup>.

The PA-18 aircraft handles quite well, especially at high-lift coefficients with the cambered plates installed. The directional stability is plentiful and the rolling performance is unchanged. In the propeller-removed gliding configuration, the aircraft could fly at approximately 9 miles per hour lower indicated airspeed than the aircraft with the square tip; and in the powered cruise condition, the loss in airspeed due to the cambered plates was less than 3 miles per hour. The possibility of the use of cambered tip plates for heavily loaded agricultural aircraft where high cruise is not of primary interest is an area worthy of further research. The cambered wing tip plates, besides increasing the performance at low speeds and high-lift coefficients, could be used to increase the effective swath width of ejected materials

by the spanwise movement of the wing tip vortices after leaving the cambered tip plate.

Other areas worthy of research in the area of induced drag are the testing of cambered wing tip plates of various sizes to complete the curves in Figures 24 and 25 and the development and testing of multi-slotted cambered tip plates similar to those used by the buzzard. Another approach is to try to utilize the energy in the wing tip vortices to drive auxiliary systems in an aircraft, such as spray pumps for agricultural aircraft, by extracting energy from the wing tip vortices by means of windmilling propellers behind the wing tips. In the case of high-lift aircraft where power could be less important than aircraft stability, perhaps spanwise blowing through a chordwise slot at the tip might be considered as well as the possibility of setting up wing tip vortices which are opposite in direction to the wing tip vortices by means of rotating circular cylinders or blowing bodies of revolution or a combination of both.

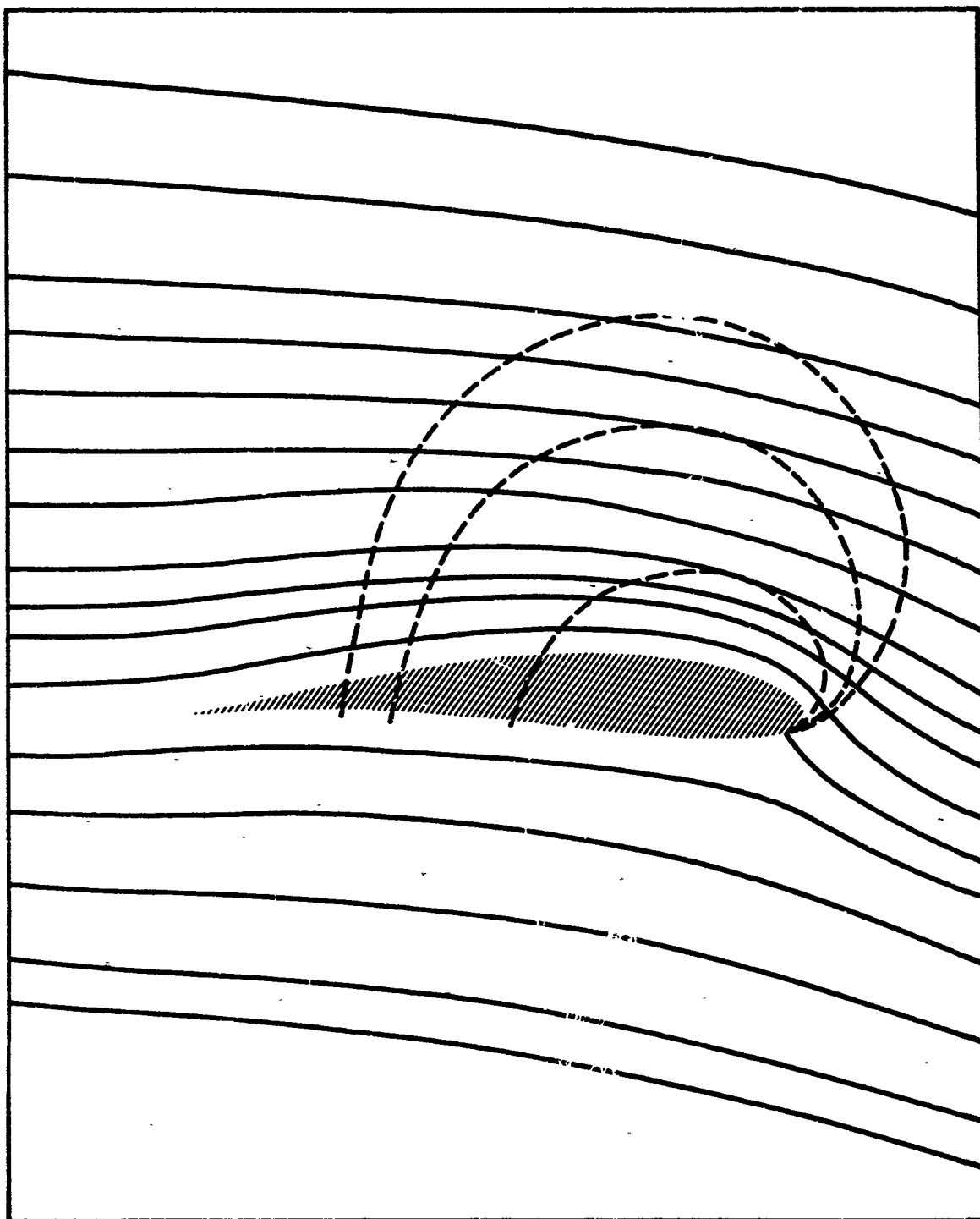


Figure 1. Plot of the Isobars About the PA-18 Airfoil Section.

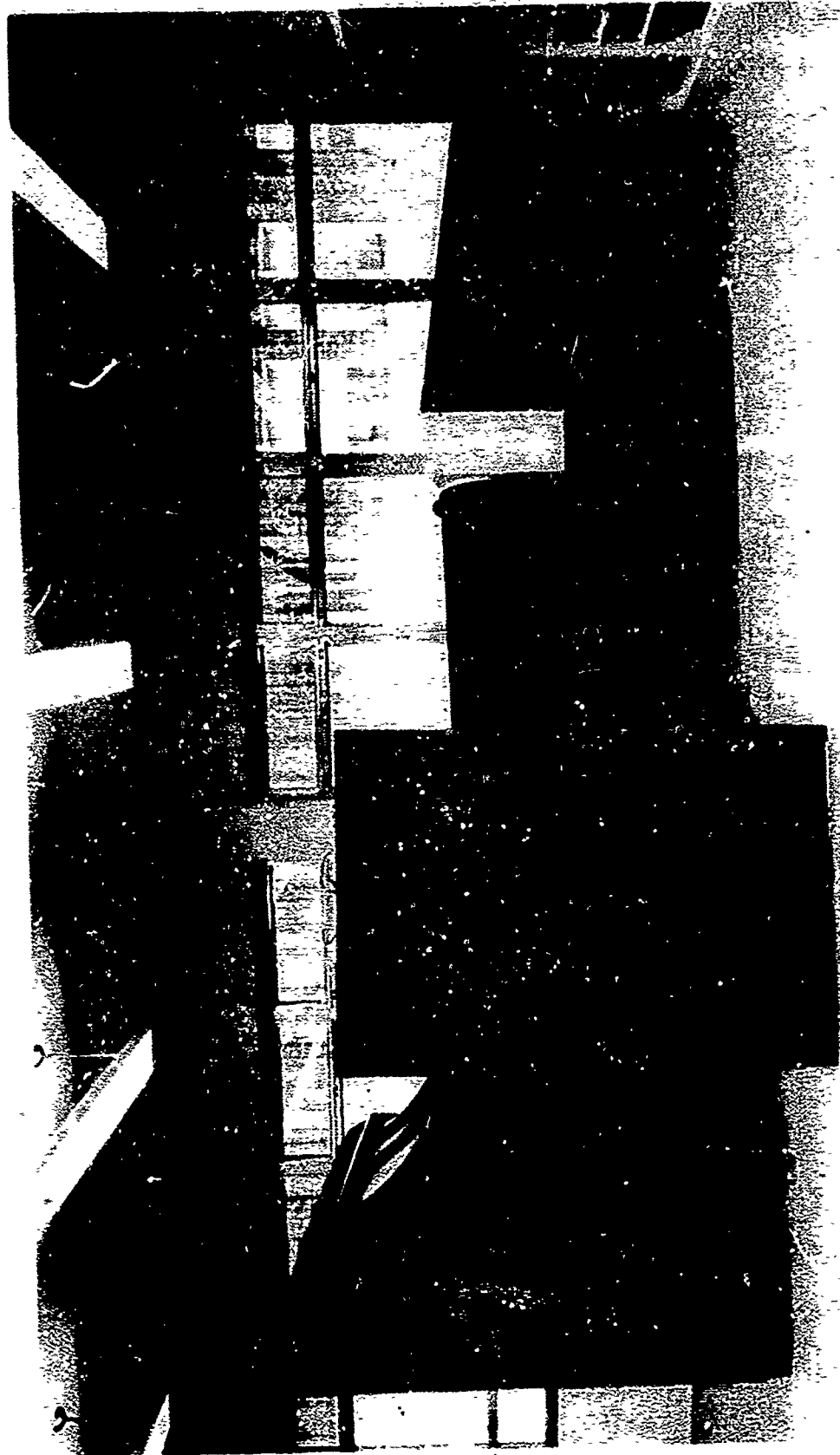


Figure 2. The Smoke Tunnel Used in the Flow Visualization Experiments.

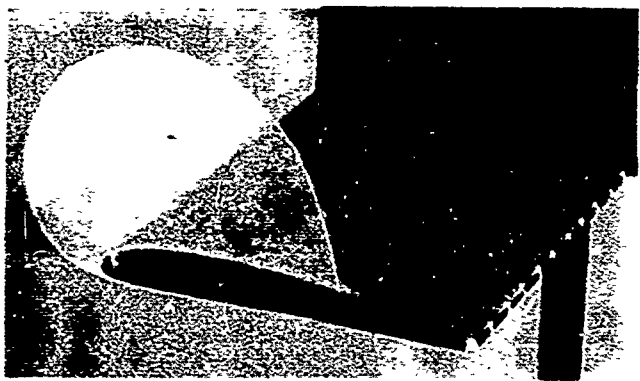
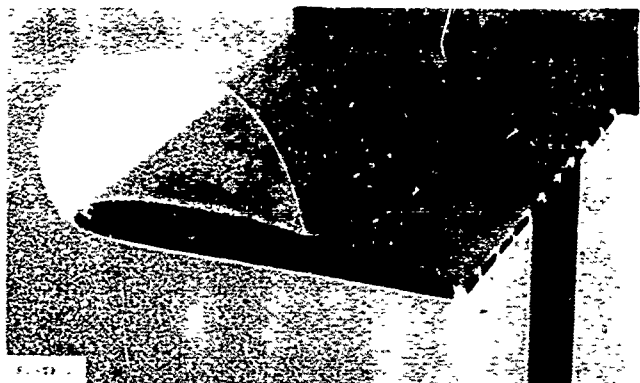
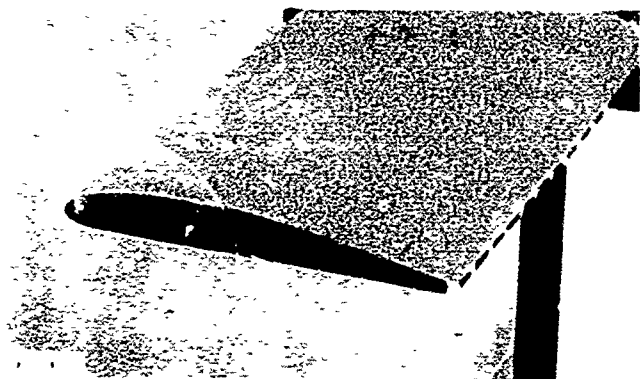
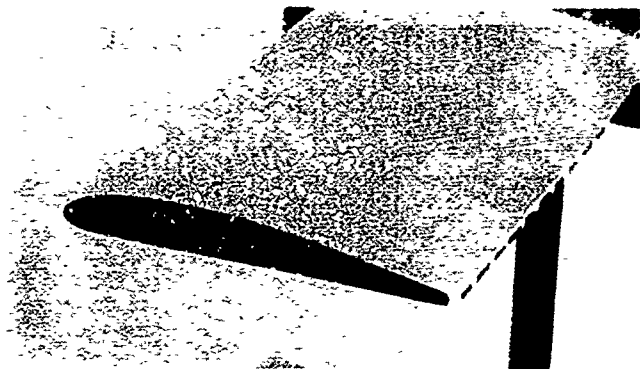


Figure 3. Model Wing With Tip Plates.

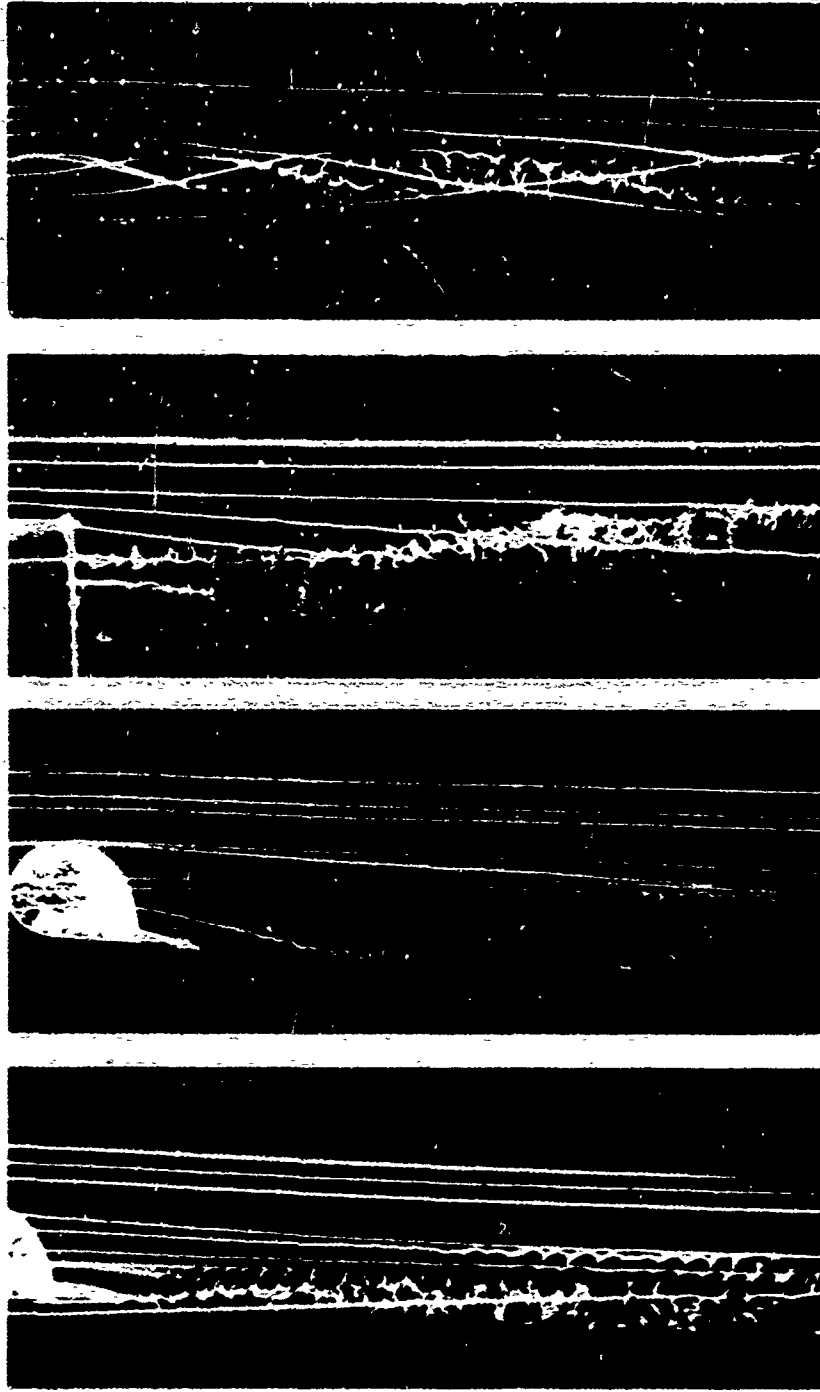


Figure 4. Smoke Photographs of Wing Tip Vortices.

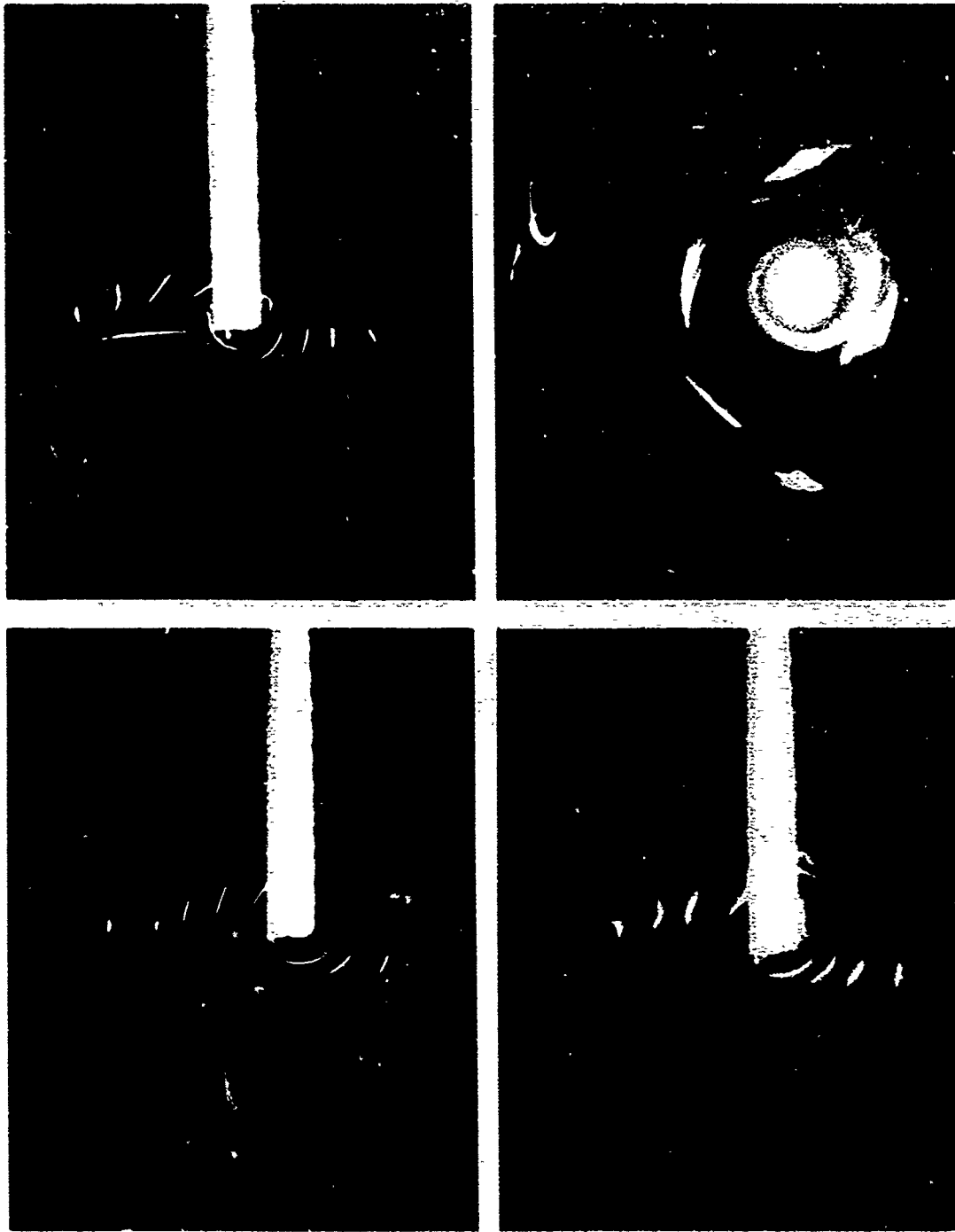


Figure 5. Typical Photographs of the Smoke Taken Axially From Behind the Vortices.

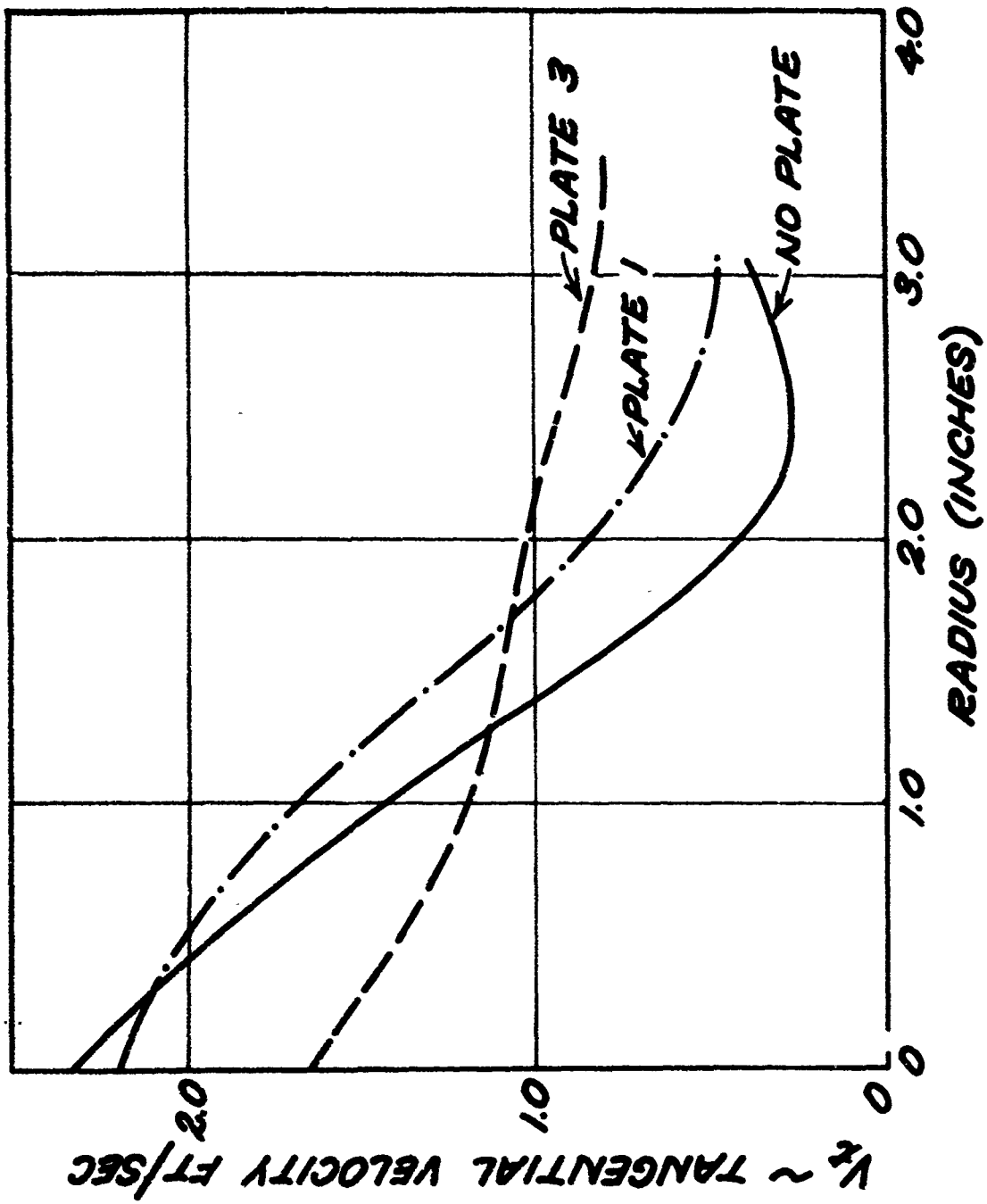


Figure 6. Tangential Velocity Profiles of the Wing Tip Vortices.

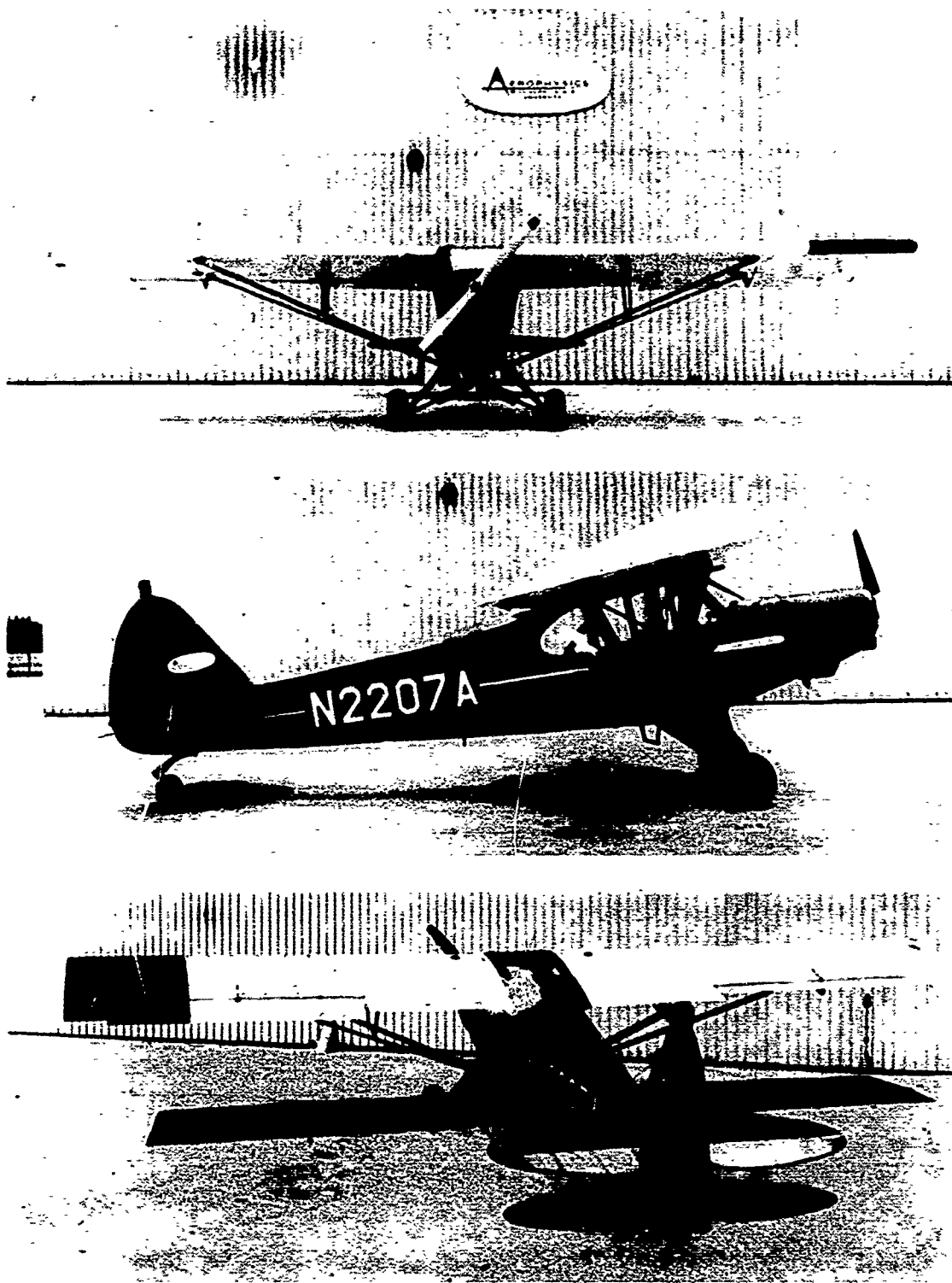


Figure 7. PA-18 Aircraft Used in the Flight Tests.

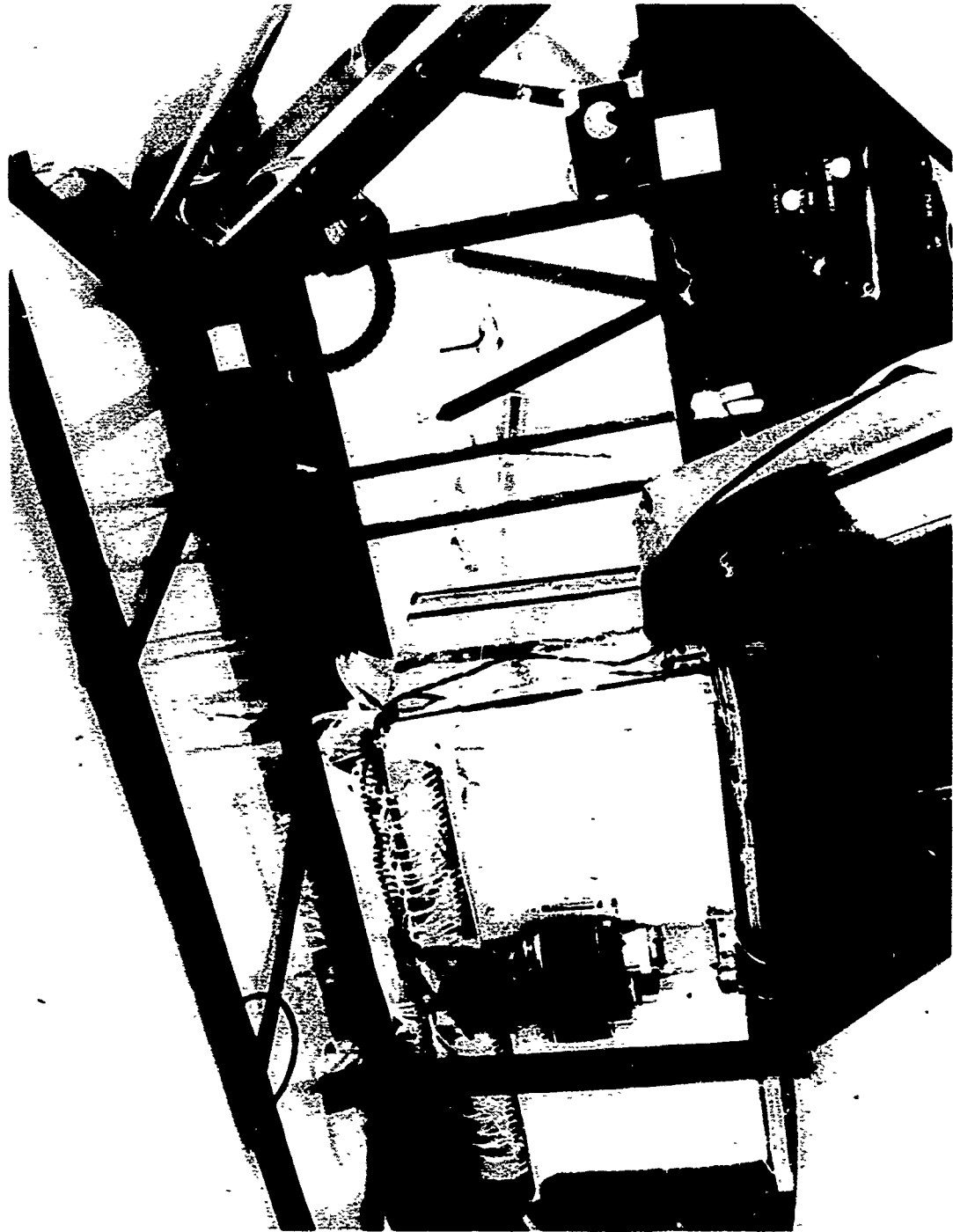


Figure 8. Installation of the Photographic Manometer in the Test Aircraft.

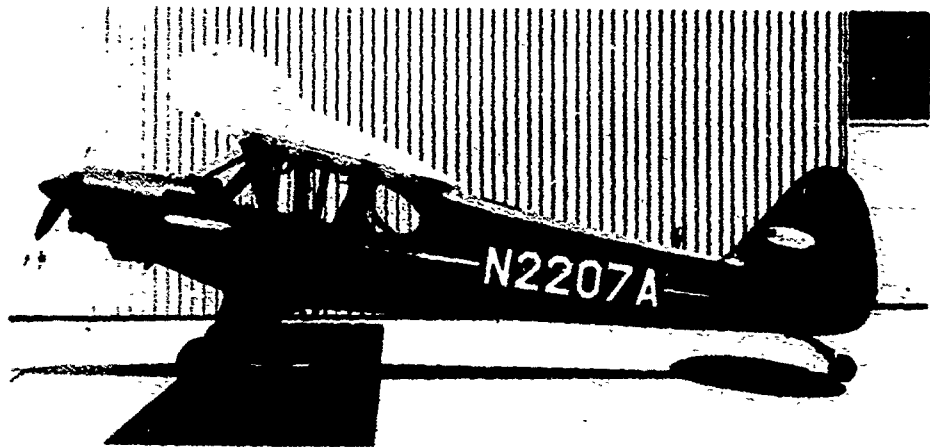
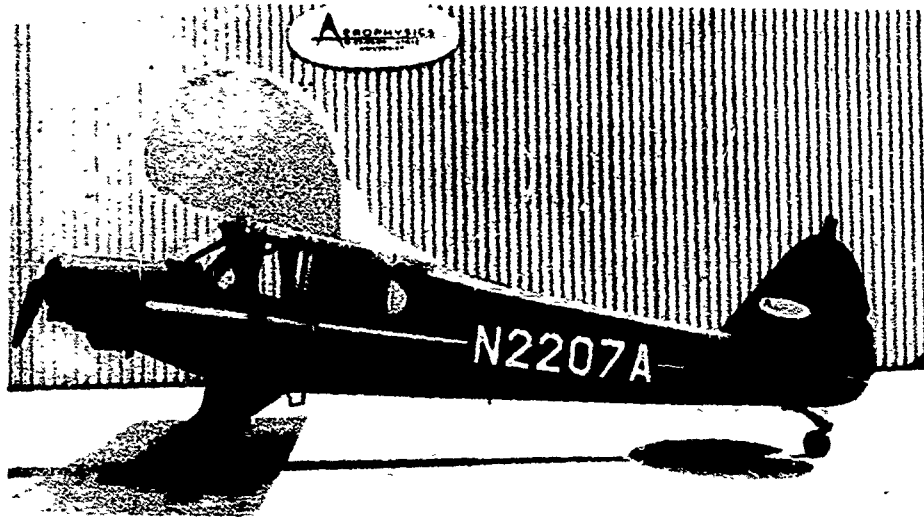
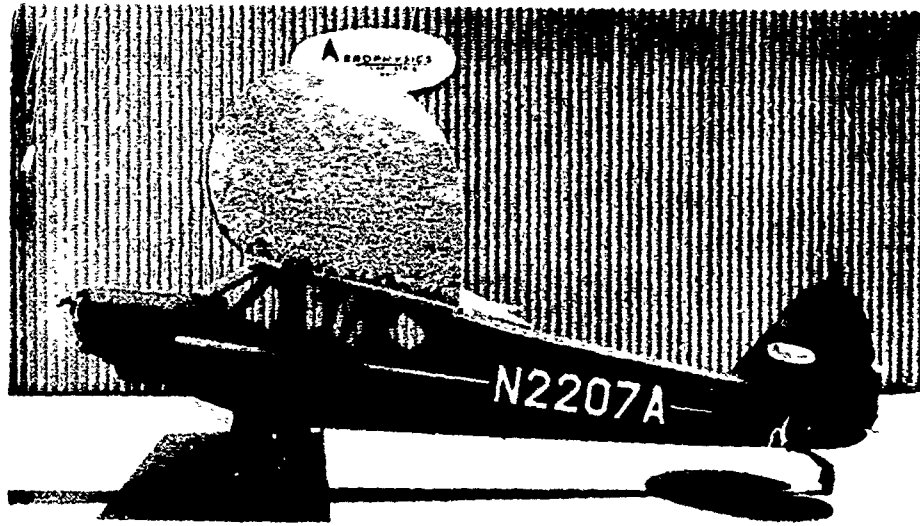


Figure 9. Flat Plate Tip Plates Tested on PA-18 Aircraft.

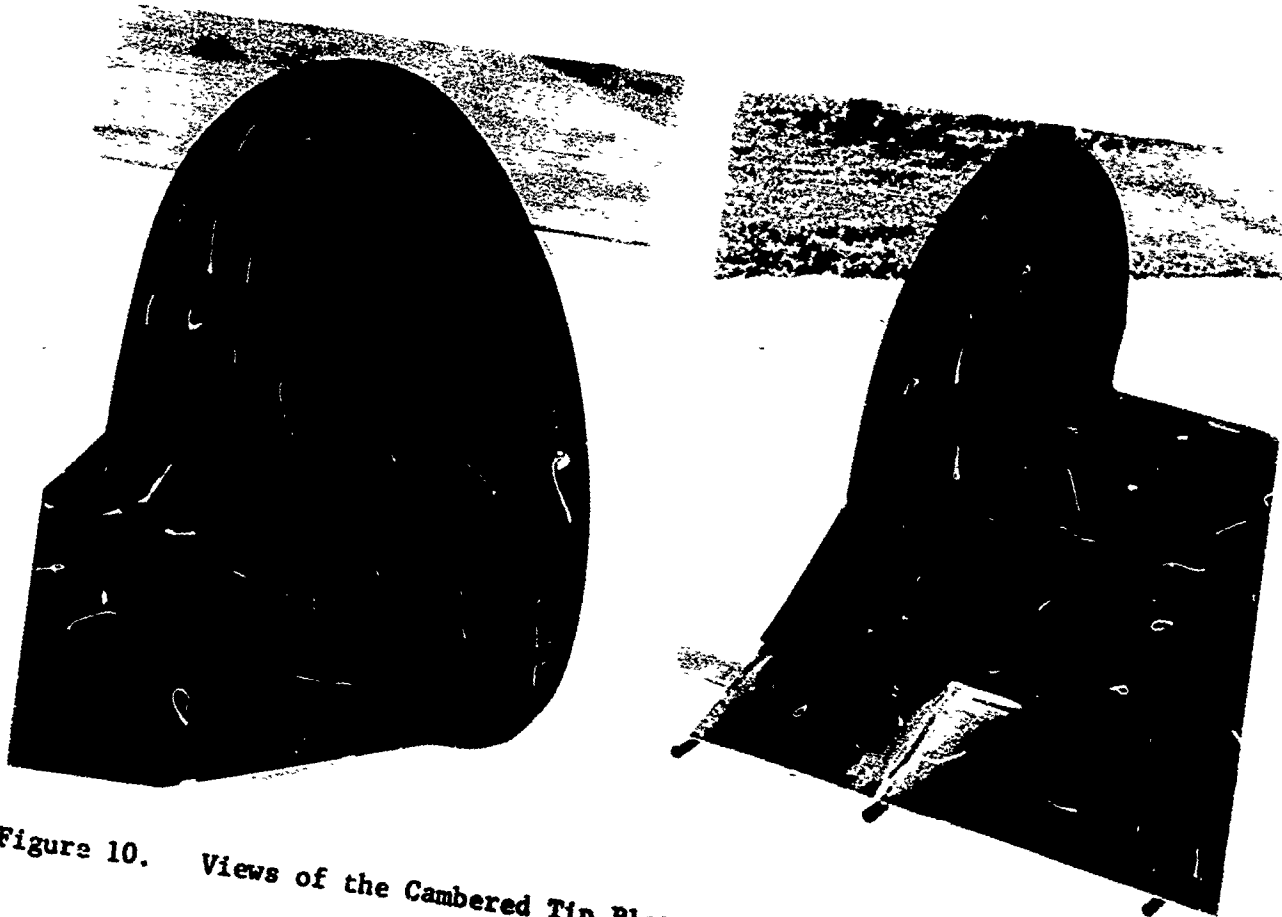


Figure 10. Views of the Cambered Tip Plates Attached to the Aircraft.

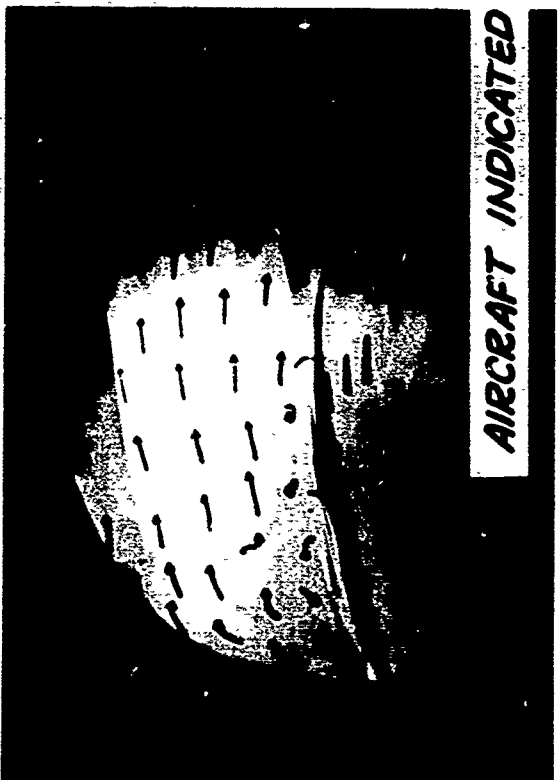


Figure 11. Tuft Pictures of the Flow at the Intersection of the Cambered Tip Plate and the Wing With and Without the Fillet.

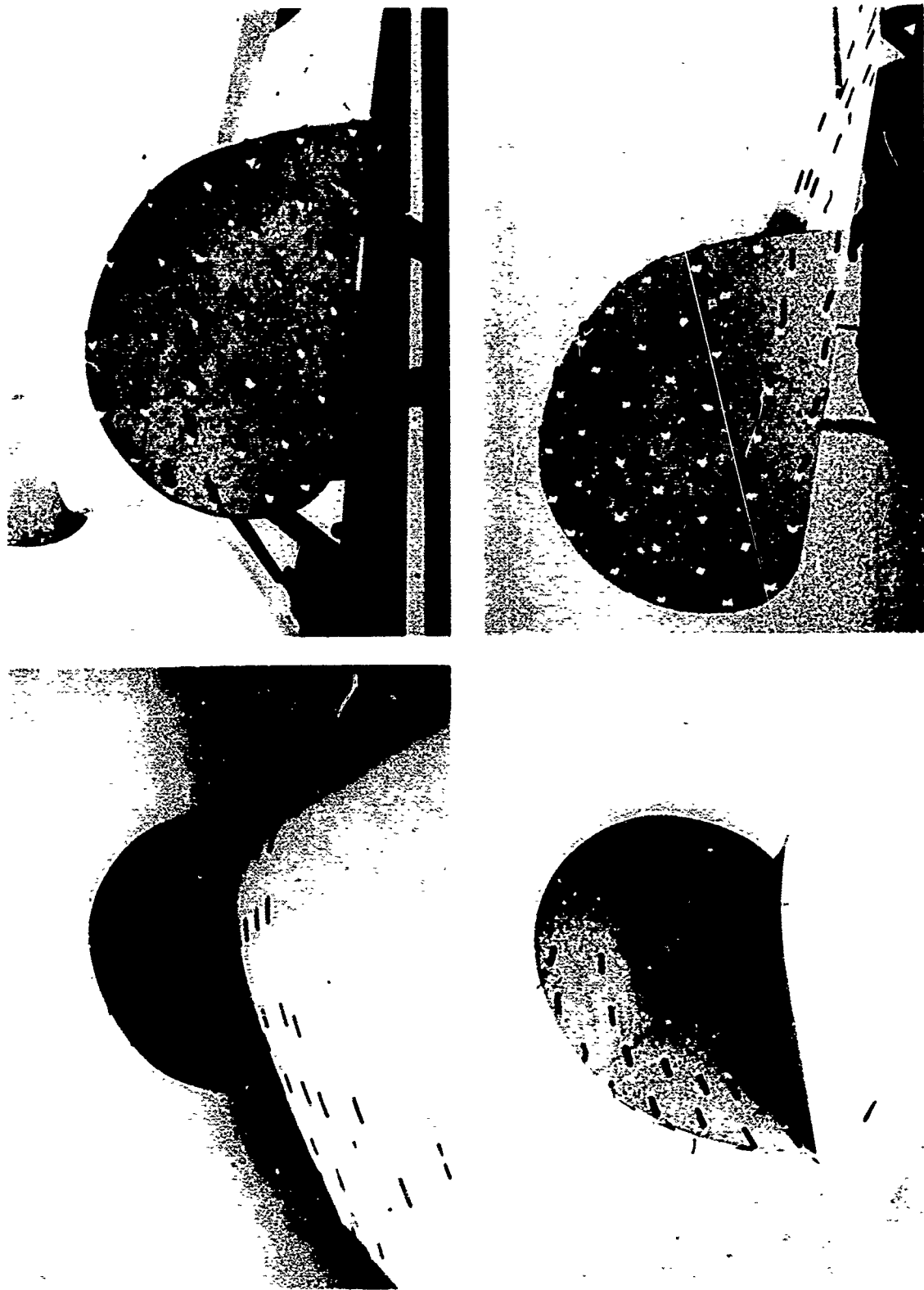


Figure 12. Tuft Pictures of the Flow About Various Tip Plates.

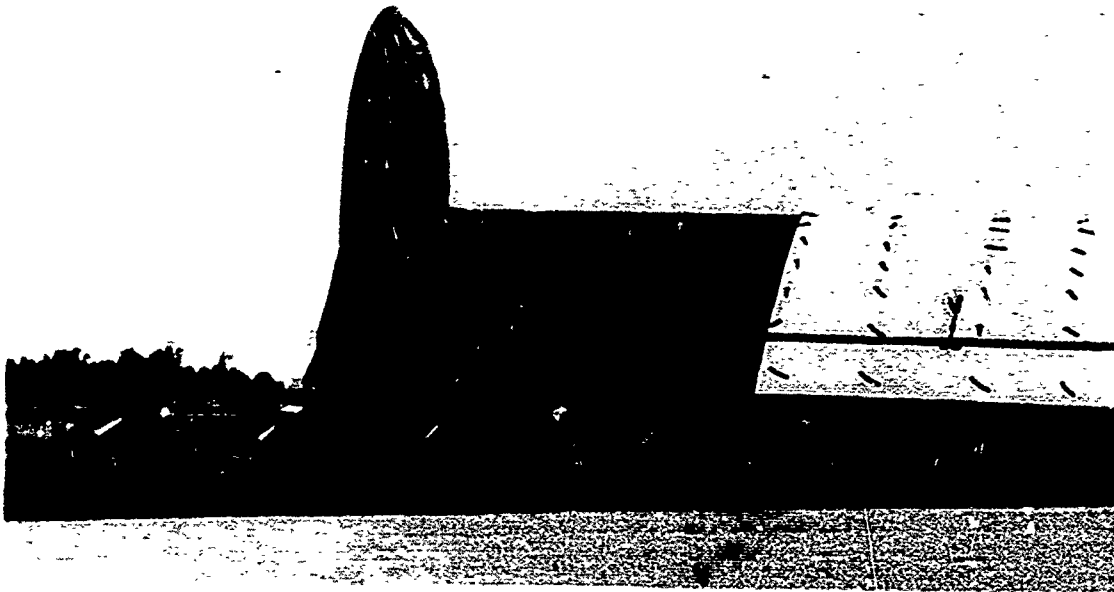
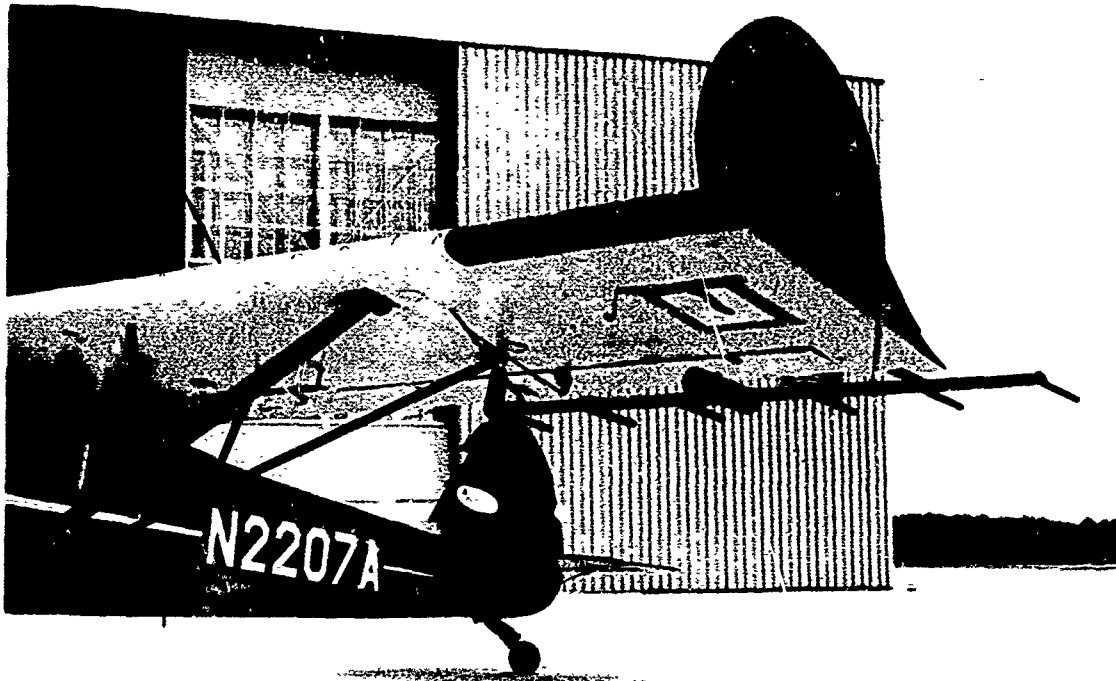


Figure 13. Smoke Rake Installation on PA-18 Aircraft.

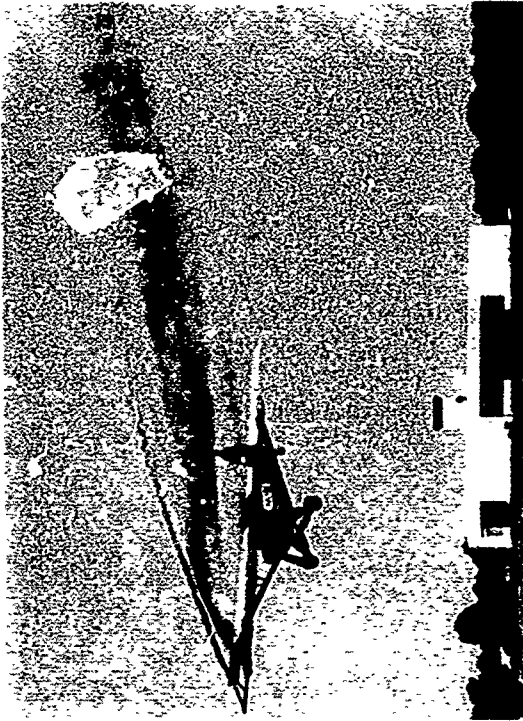


Figure 14a. Typical Flow Patterns Behind the Wing Tips With No Tip Plates.



Figure 14b. Flow Patterns Behind the Wing Tips With the Cambered Tip Plates.

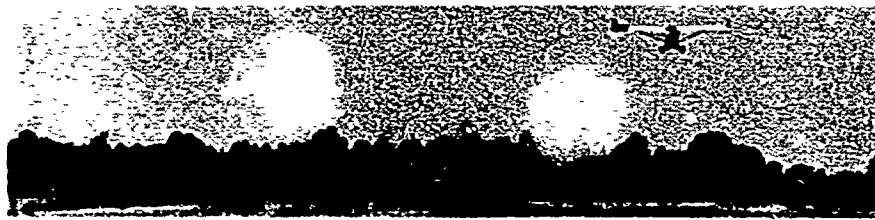
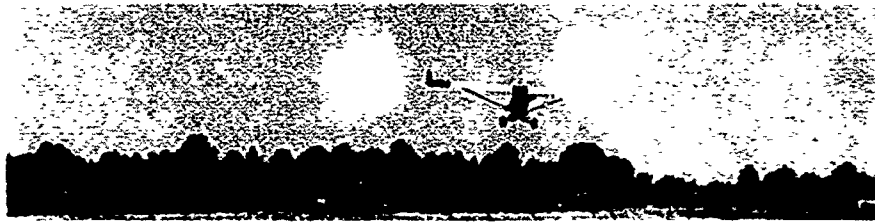
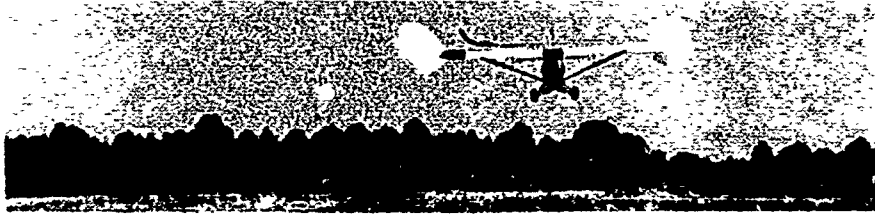


Figure 15. Typical Series of Dust Bomb Photographs.

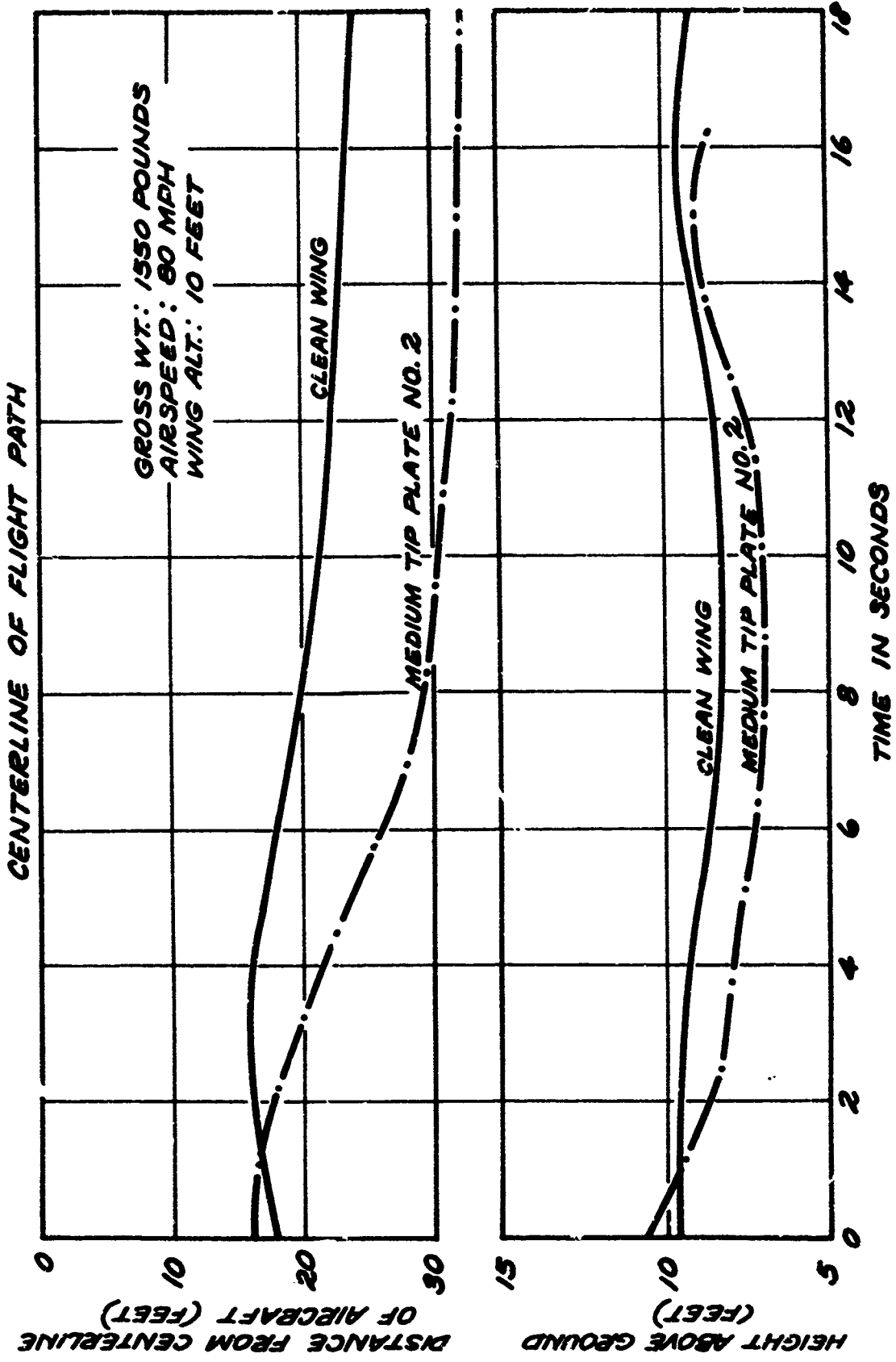


Figure 16. Effect of End Plates on the Wing Tip Vortices.

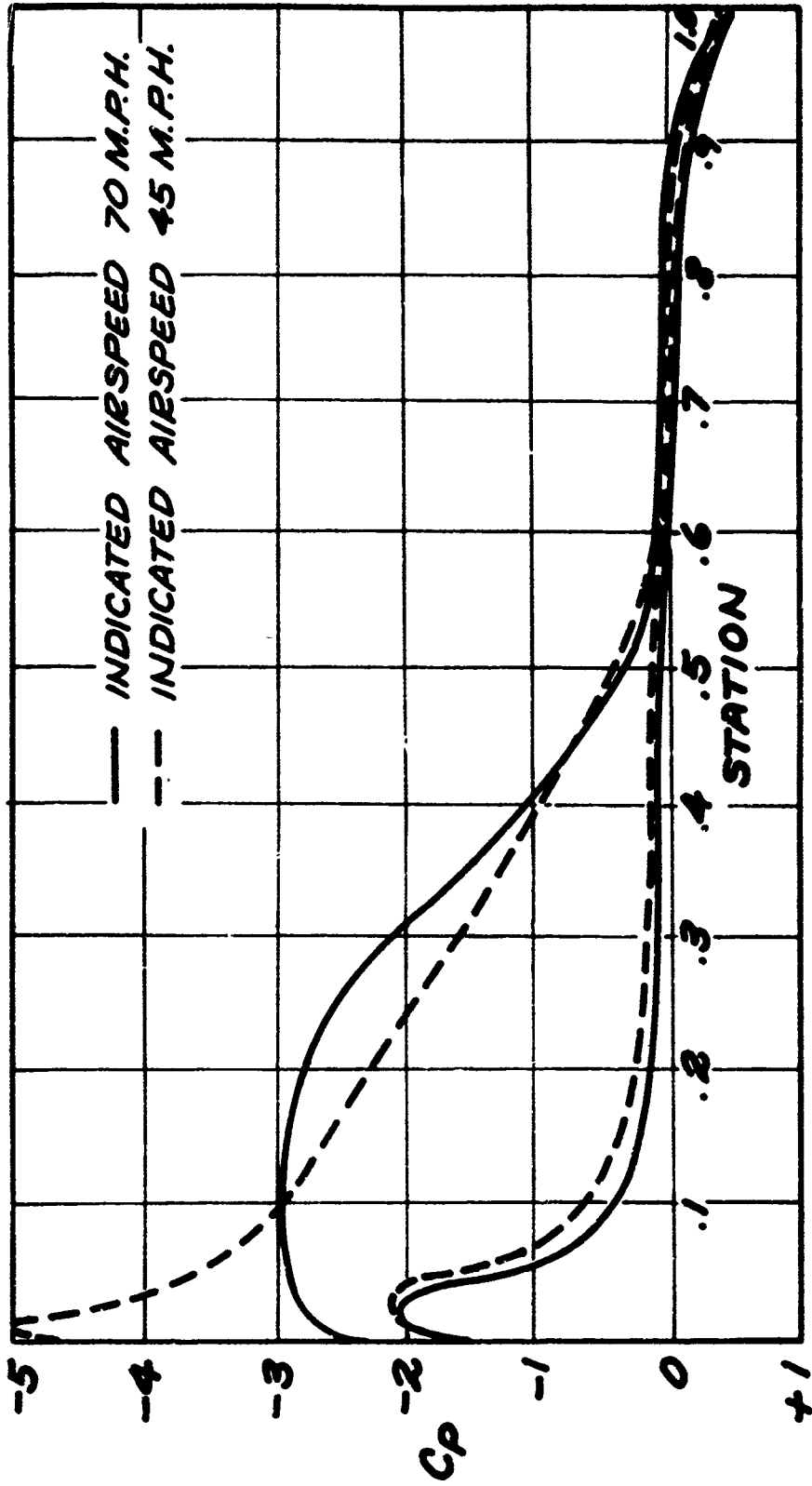


Figure 17. Typical Chordwise Pressure Distributions.

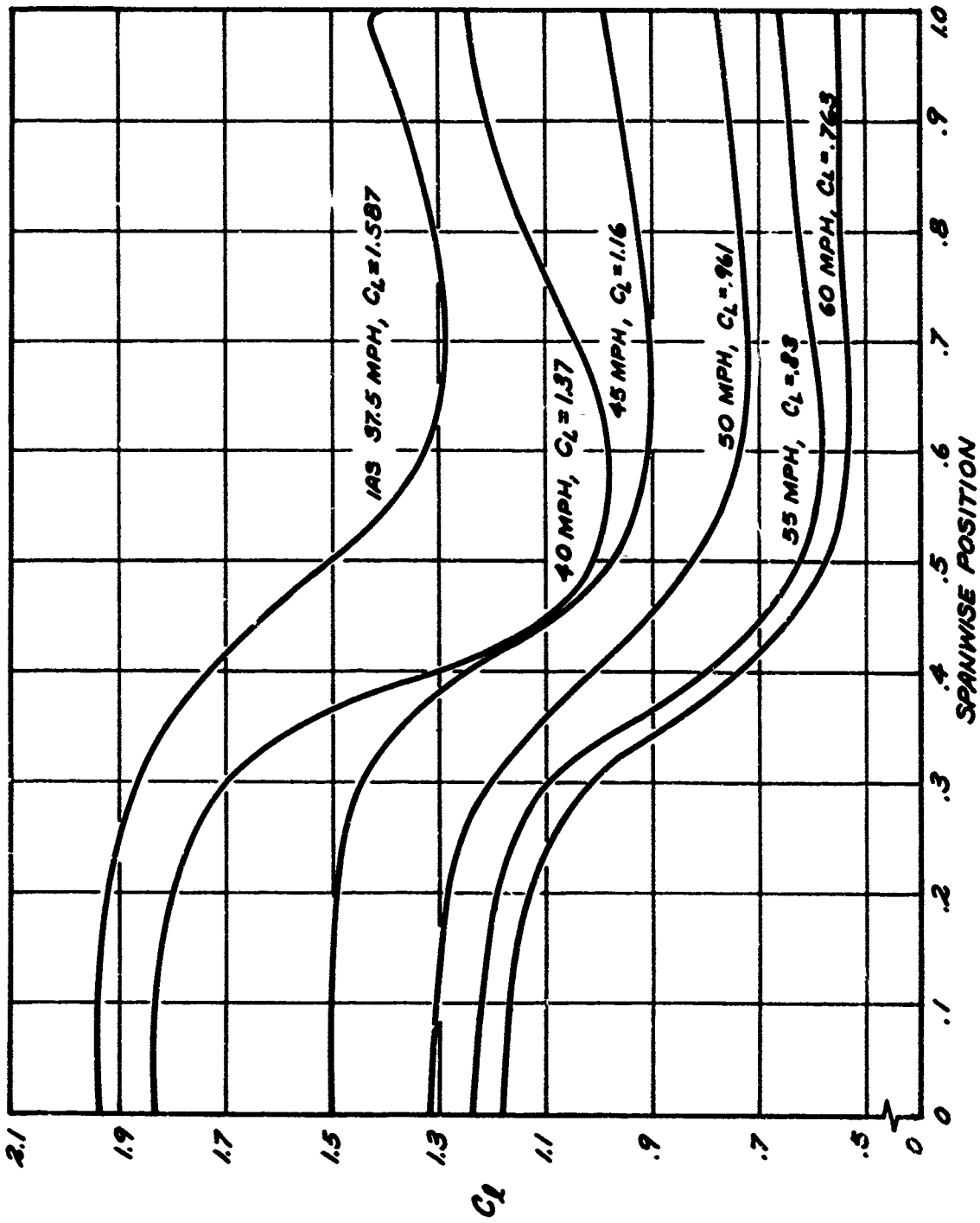


Figure 18. Typical Spanwise Loading Curves for Various Aircraft Airspeeds.

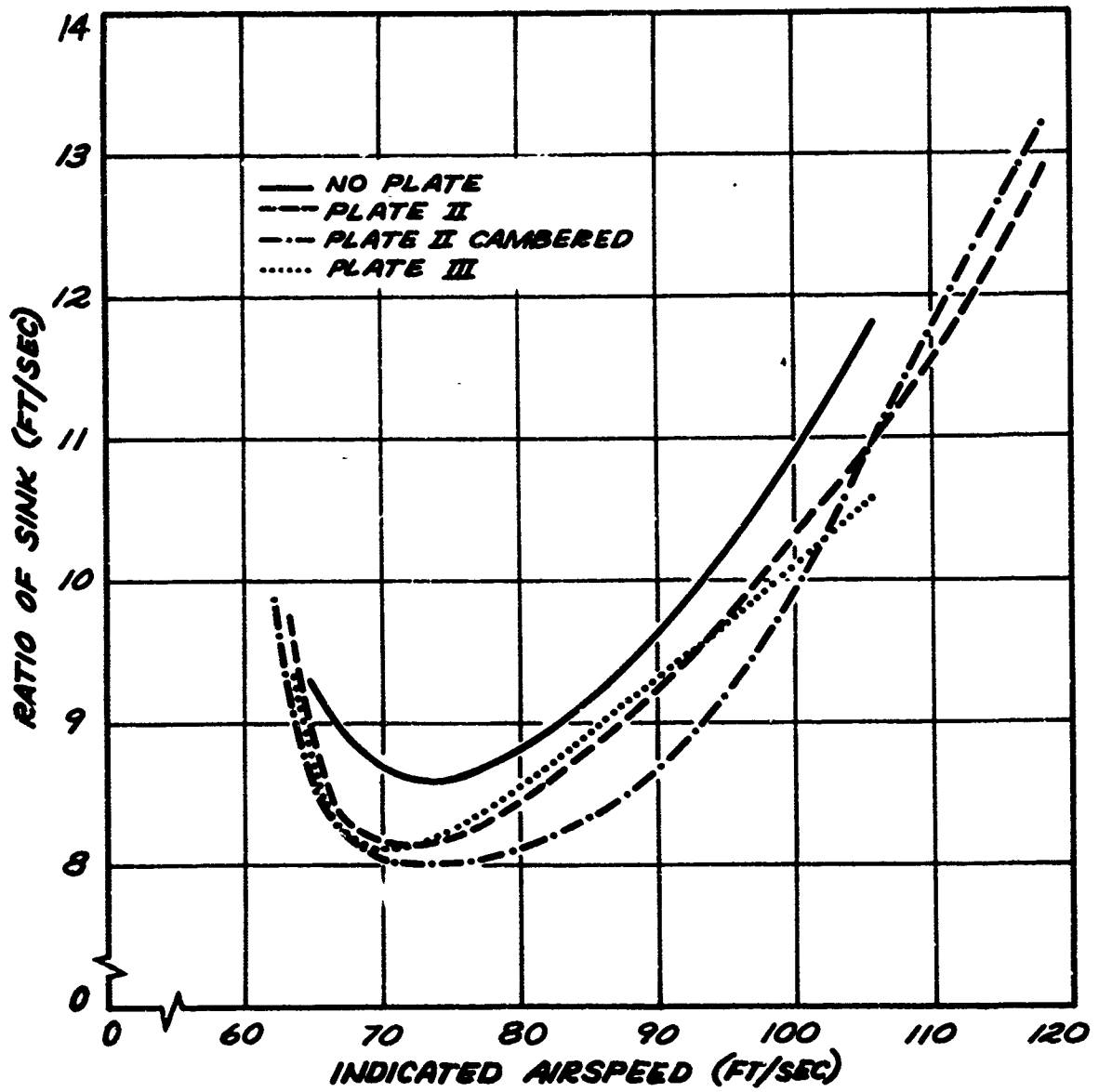


Figure 19. Typical Rate of Sink Results for the PA-18 Aircraft With Various Tip Configurations.

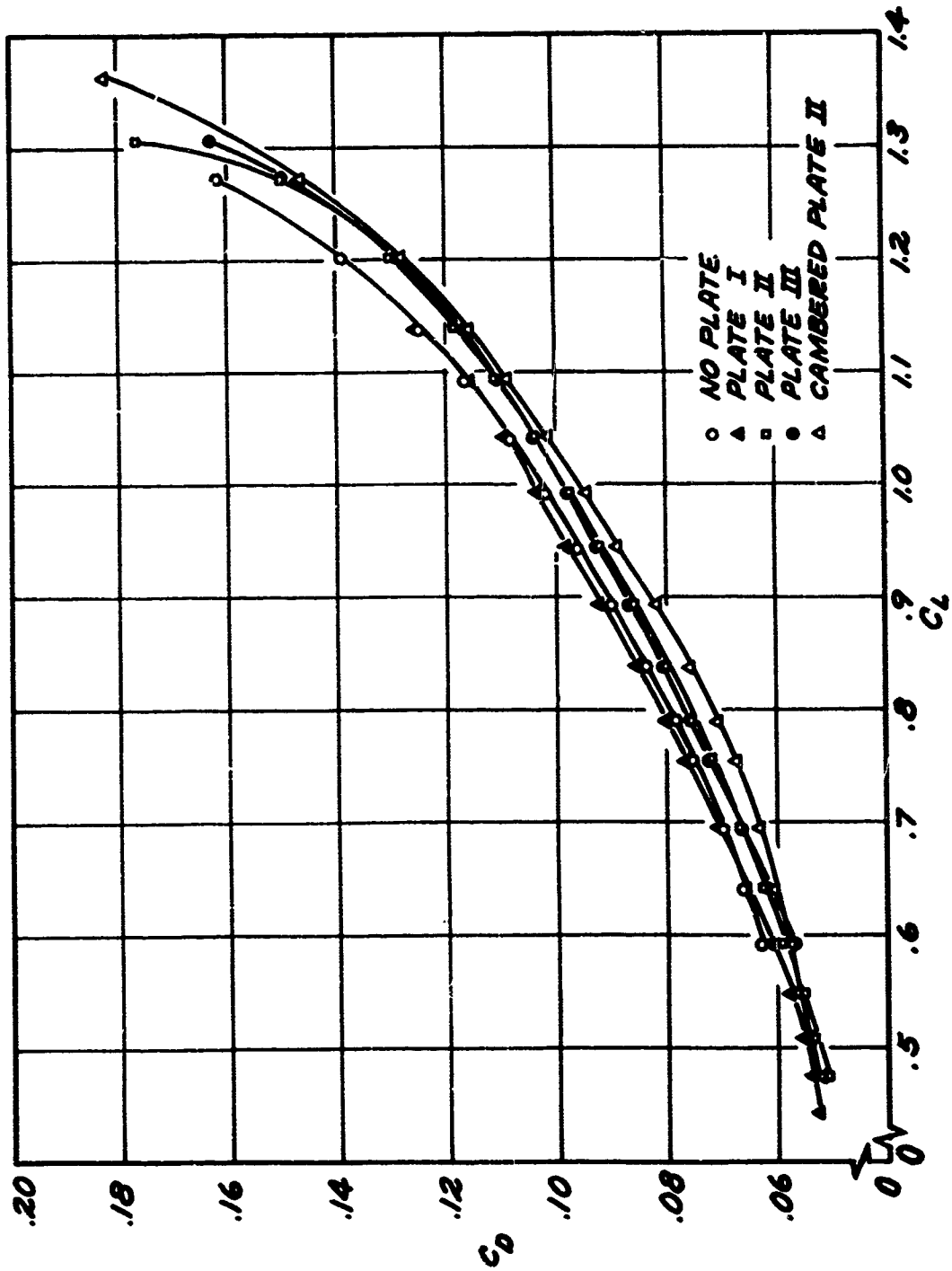


Figure 20a. Drag Polars of the PA-18 Aircraft With Various Tip Configurations With No Flaps.

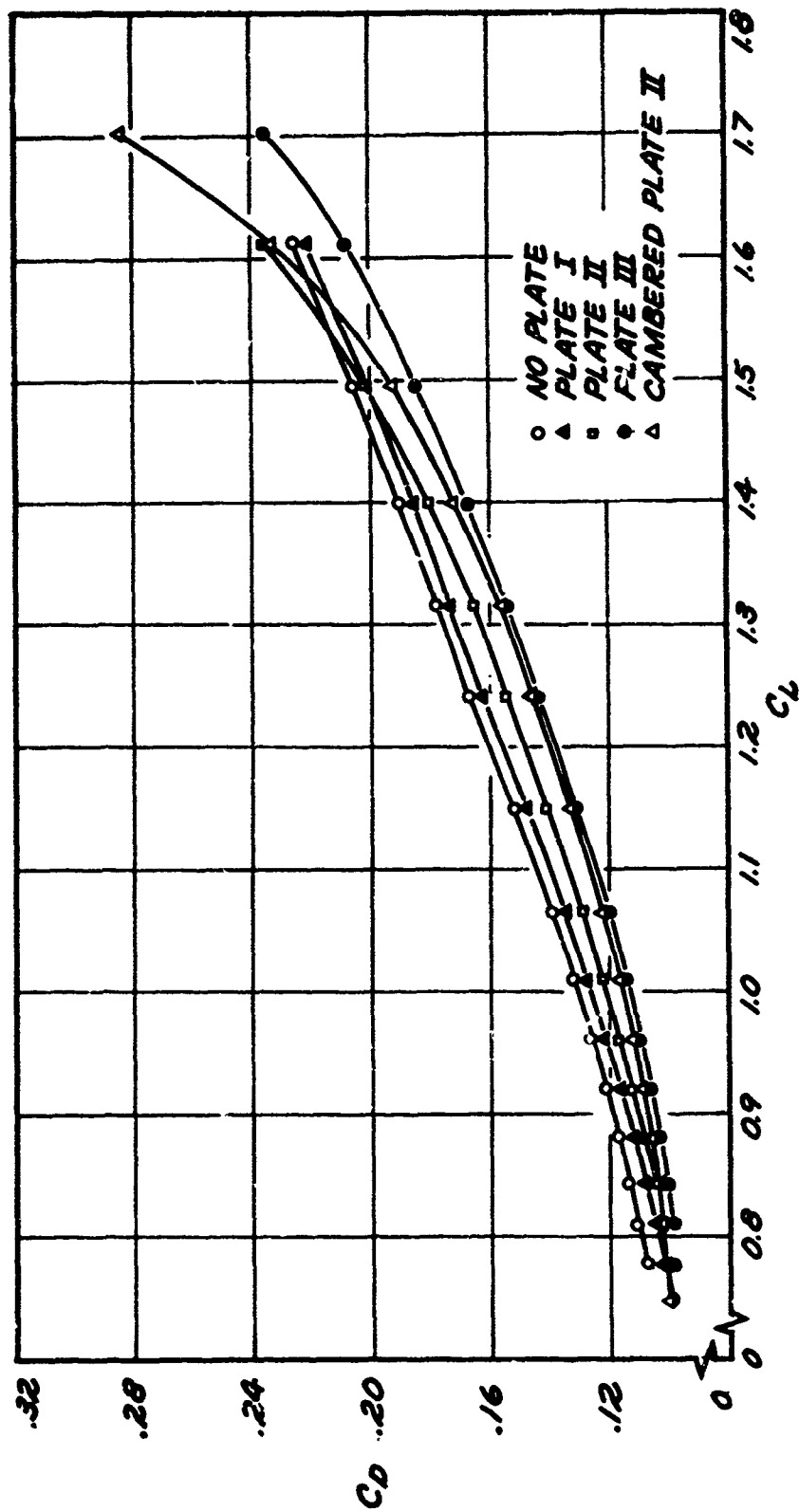


Figure 20b. Drag Polars of the PA-18 Aircraft With Various Tip Configurations With Full Flaps.

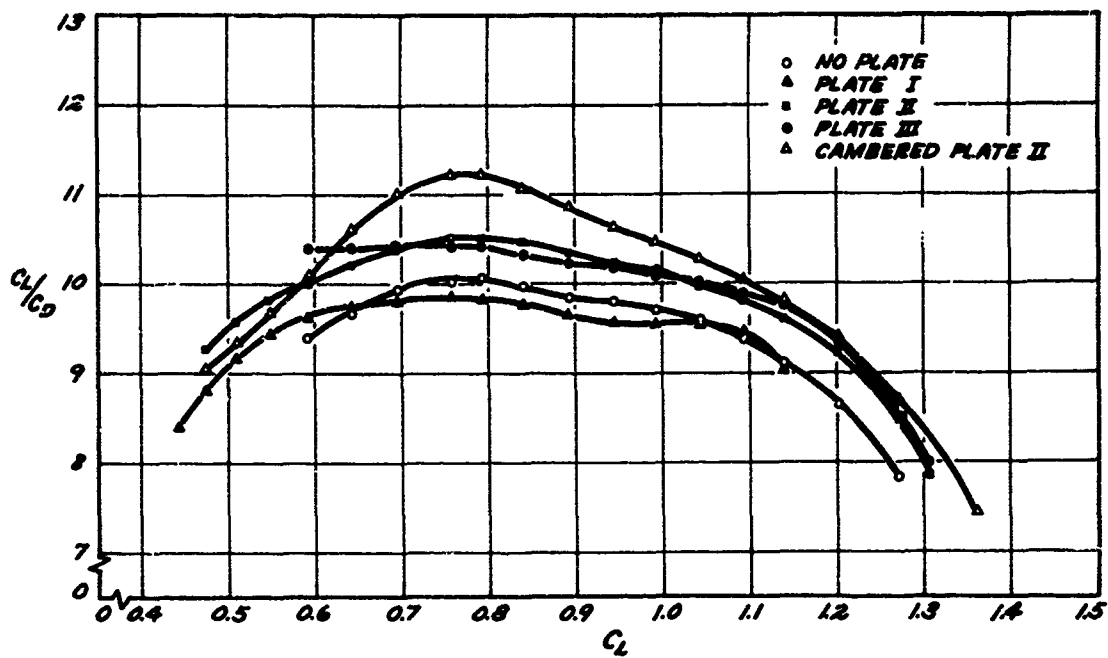


Figure 21a. Lift to Drag Ratios of the PA-18 Aircraft With Various Tip Configurations as a Function of Lift Coefficient With No Flaps.

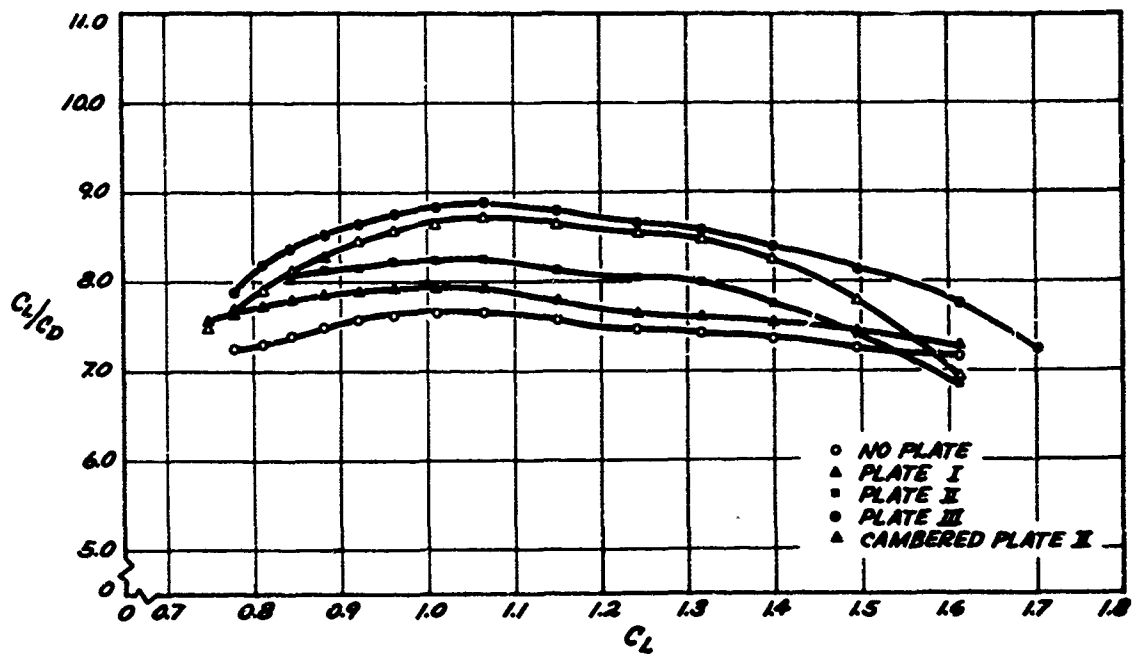


Figure 21b. Lift to Drag Ratios of the PA-18 Aircraft With Various Tip Configurations as a Function of Lift Coefficient With Full Flaps.

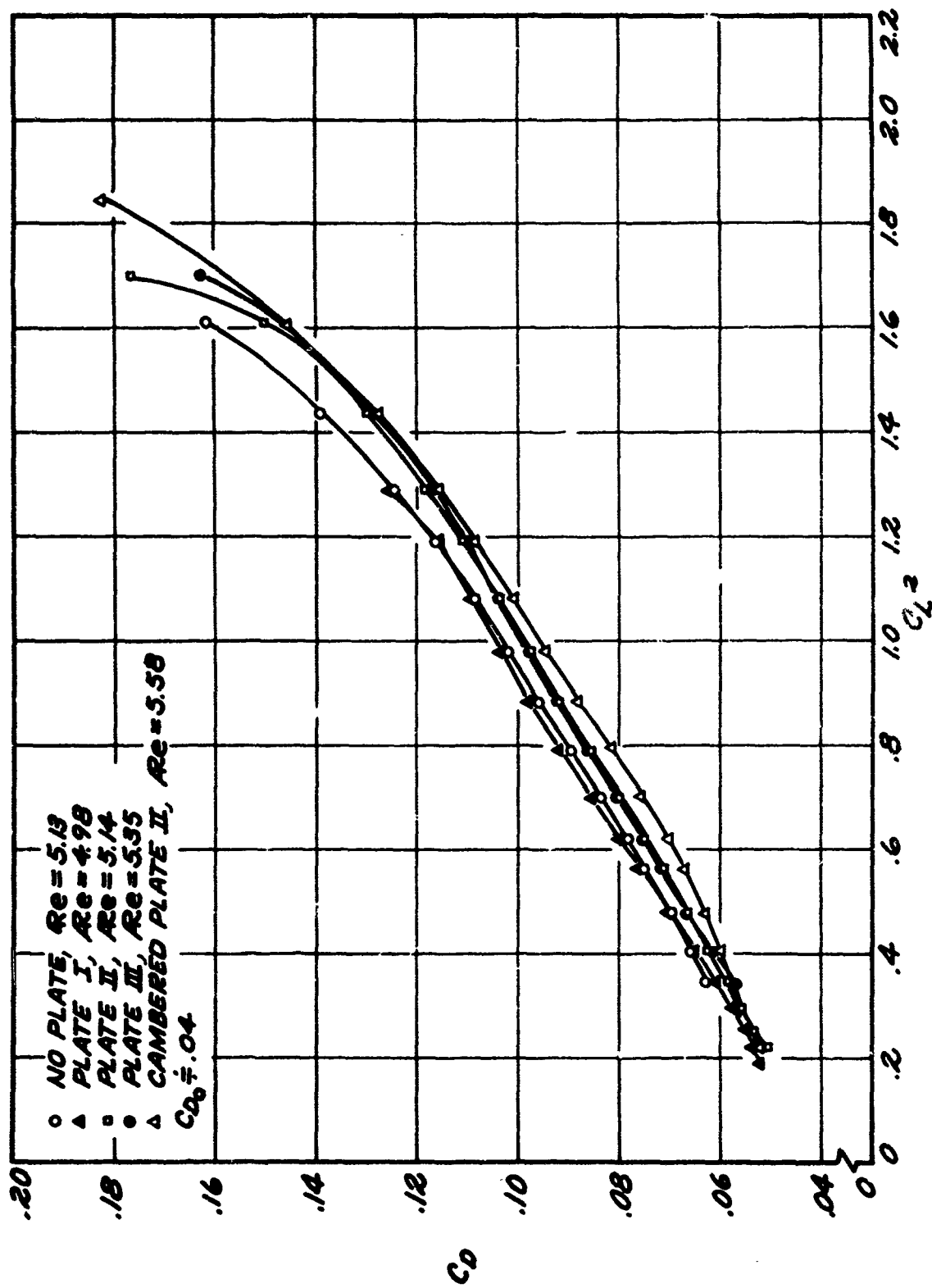


Figure 22a. Plots of  $C_D$  vs  $C_L^2$  for Various Wing Tip Configurations With No Flaps.

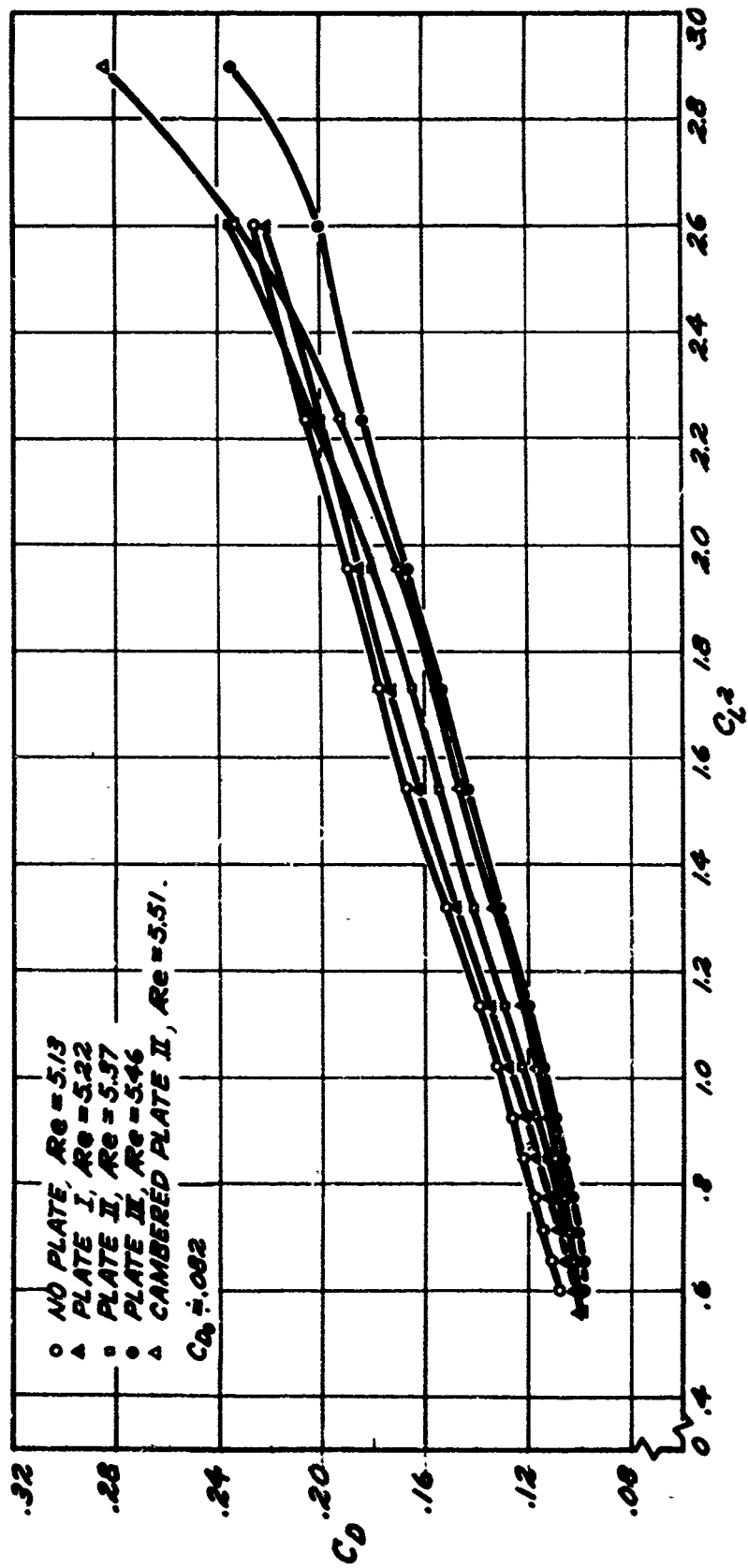


Figure 22b. Plots of  $C_D$  vs  $C_L^2$  for Various Wing Tip Configurations With Full Flaps.

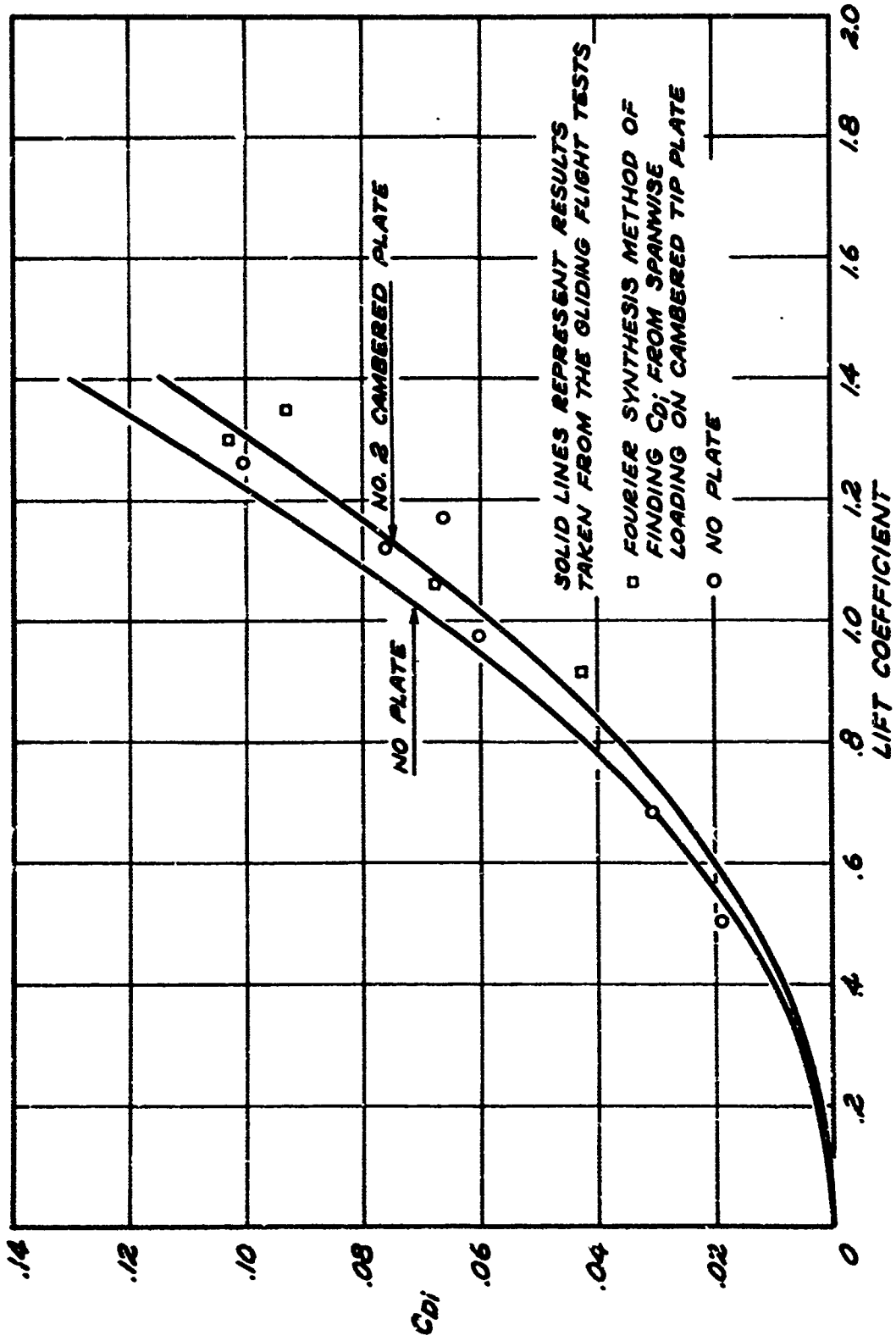


Figure 23. Effect of Cambered End Plates on Induced Drag Coefficient.

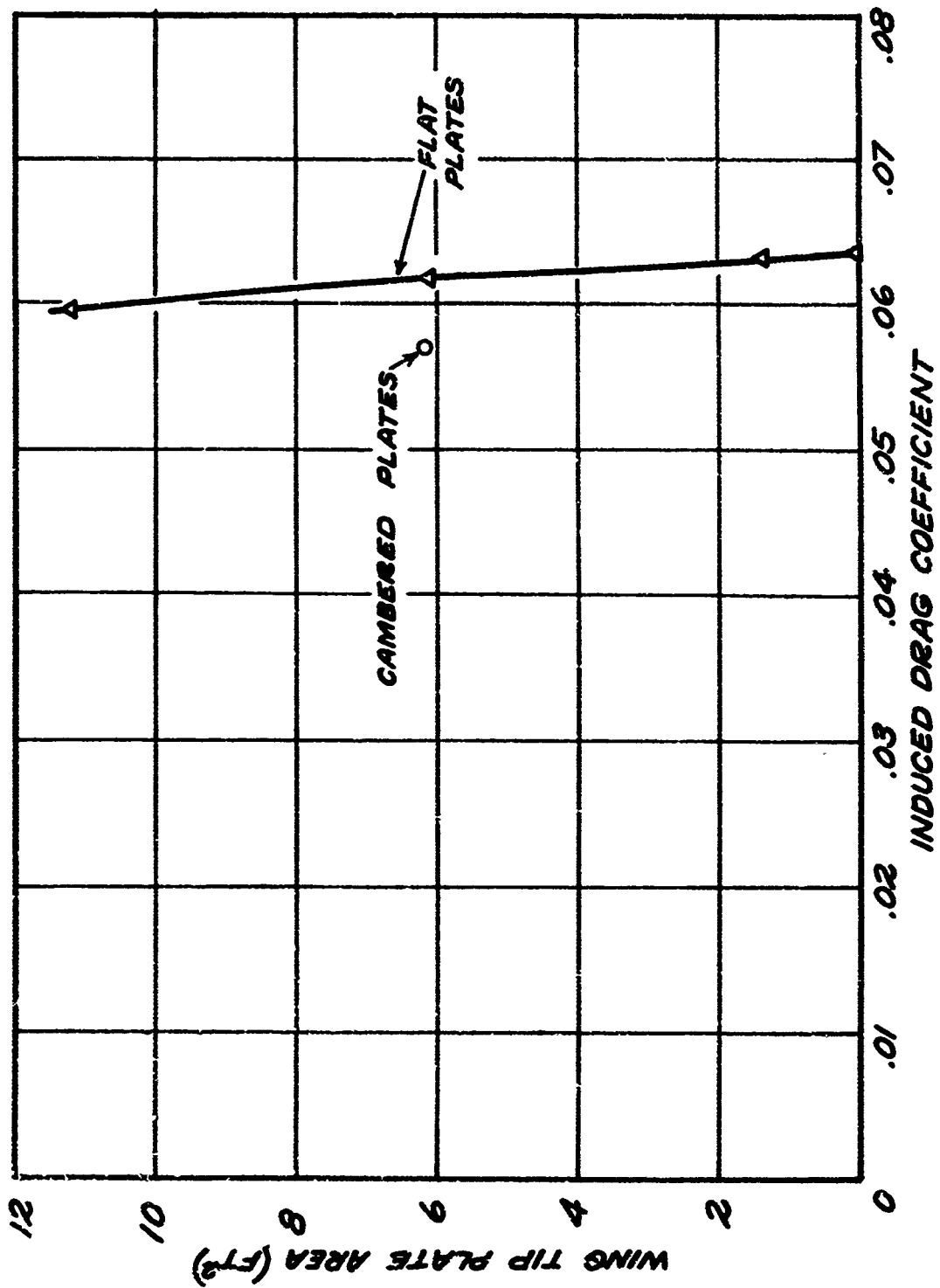


Figure 24. Plot of Plate Area Against Induced Drag Coefficient,  $C_L = 1.0$ .

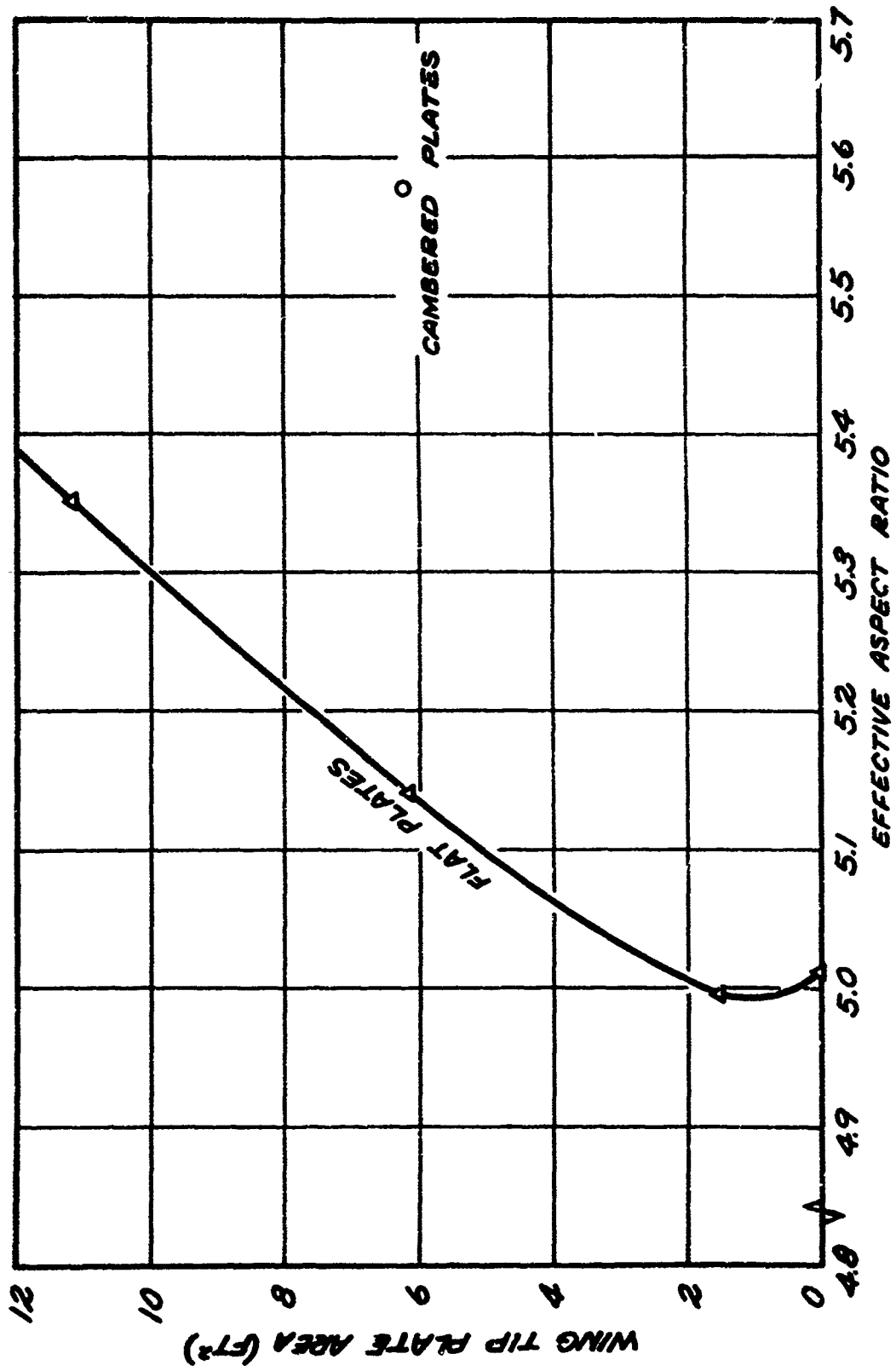


Figure 25. Plot of Plate Area Against Effective Aspect Ratio.

#### REFERENCES

1. Cone, Clarence D., Jr., A Theoretical Investigation of Vortex Speed Deformation Behind a Highly Loaded Wing and Its Effect on Lift, NASA TND 657, April 1961.
2. Cone, Clarence D., Jr., The Aerodynamic Design of Wings With Cambered Span Having Minimum Induced Drag, NASA TRR 152, 1963.
3. Cone, Clarence D., Jr., "The Soaring Flight of Birds", Scientific American, April 1962, p. 130.
4. Cone, Clarence D., Jr., The Theory of Induced Lift and Minimum Induced Drag of Nonplanar Lifting Systems, NASA TRR 139, 1962.
5. Cone, Clarence D., Jr., "Thermal Soaring of Birds", American Scientist, March 1962, p. 180.
6. Cornish, J. J., III, and Wells, G. W., "Boundary Layer Control Applications to Man-Powered Flight", Canadian Aeronautics and Space Journal, Volume 9, Number 2, February 1963.
7. Hoerner, S. F., Fluid Dynamic Drag, published by the author, 1958.
8. Raspert, August, Biophysics of Birds, Aerophysics Department, Mississippi State University, State College, Mississippi, 1960.
9. Raspert, August, "Performance Measurements of a Soaring Bird", Aeronautical Engineering Review, Volume 9, Number 12, December 1950.
10. Roberts, S. C., and Smith, M., A Flight Test Analysis of a Positive Energy Distribution System on an Agricultural Stearman, Aerophysics Department, Mississippi State University, State College, Mississippi, Research Report No. 52, March 1964.
11. Roberts, S. C., and Smith, M., Flow Visualization Techniques Used in Full Scale Flight Tests, Aerophysics Department, Mississippi State University, State College, Mississippi, Research Report No. 49, April 1964.
12. Roberts, S. C., and Smith, M., The Evaluation of a Positive Energy Distribution System for the Aerial Application of Solid Materials, Aerophysics Department, Mississippi State University, State College, Mississippi, Research Note No. 20, February 1964.

## DISTRIBUTION

US Army Materiel Command	6
US Army Mobility Command	3
US Army Aviation Materiel Command	5
United States Continental Army Command, Fort Rucker	2
Chief of R&D, DA	1
US Army Aviation Materiel Laboratories	12
US Army R&D Group (Europe)	2
US Army Limited War Laboratory	1
US Army Research Office-Durham	1
US Army Test and Evaluation Command	1
US Army Medical R&D Command	1
US Army Engineer Waterways Experiment Station	1
US Army Combat Developments Command, Fort Belvoir	2
US Army Combat Developments Command Experimentation Command	3
US Army Command and General Staff College	1
US Army Transportation School	1
US Army Aviation School	1
US Army Infantry Center	2
US Army Aviation Maintenance Center	2
US Army Aviation Test Board	3
US Army Electronics Command	2
US Army Aviation Test Activity	2
Air Force Flight Test Center, Edwards AFB	1
US Army Field Office, AFSC, Andrews AFB	1
Air Force Flight Dynamics Laboratory, Wright-Patterson AFB	1
Systems Engineering Group (RTD), Wright-Patterson AFB	2
Bureau of Ships, DN	1
Bureau of Naval Weapons, DN	6
Office of Naval Research	2
Chief of Naval Research	2
US Naval Air Station, Norfolk	1
David Taylor Model Basin	1
Commandant of the Marine Corps	1
Ames Research Center, NASA	1
Lewis Research Center, NASA	1
Manned Spacecraft Center, NASA	1
NASA Representative, Scientific and Technical Information Facility	2
Research Analysis Corporation	1
NAFEC Library (FAA)	2
US Army Board for Aviation Accident Research	1
Bureau of Safety, Civil Aeronautics Board	2
US Naval Aviation Safety Center	1
Federal Aviation Agency, Washington, D. C.	1
The Surgeon General	1
Defense Documentation Center	20

APPENDIX I

PROCEDURE FOR THE MATHEMATICAL DETERMINATION OF  
ISOBARS ABOUT AN ARBITRARY AIRFOIL SECTION

- A. Procedure for the determination of a circle to be transformed into a Joukowski airfoil:

C = chord of given airfoil

T = thickness of given airfoil

$$\epsilon = 0.77 \frac{T}{C}, \quad C_1 = \frac{C}{4(1+\epsilon^2)} \doteq \frac{C}{4}$$

$$a = C_1(1+\epsilon)$$

$$me^{i\delta} = -C_1 + ae^{i\beta}$$

- B. Now the circle is transformed by the Joukowski transformation,

$$\zeta = z + \frac{C^2}{z}$$

$$\xi = x \left[ 1 + \frac{C_1^2}{x^2 + y^2} \right]$$

$$\eta = y \left[ 1 - \frac{C_1^2}{x^2 + y^2} \right]$$

- C. If  $W$  = weight of aircraft  
And  $S_w$  = wing area of aircraft  
Given a value of lift coefficient,  $C_L$ :

$$C_L = \frac{W}{\frac{1}{2} \rho U_\infty^2 S_w}$$

$$U_\infty = \sqrt{\frac{2W}{S_w C_L}}$$

$$C_L = \frac{2\pi(1+\epsilon)}{(1+\epsilon^2)} \sin(\alpha + \beta)$$

$$\sin(\alpha + \beta) = \frac{C_L(1 + \epsilon^2)}{2\pi(1 + \epsilon)} \quad \epsilon^2 \text{ is negligible}$$

$$\alpha = \arcsin \frac{C_L}{2\pi(1 + \epsilon)} - \beta \quad \alpha \text{ is determined}$$

$$C_L = \frac{2\pi(1 + \epsilon)}{(1 + \epsilon^2)} \sin(\alpha + \beta)$$

$$= 2\pi \frac{a}{c_1} \sin(\alpha + \beta)$$

$$K = 4\pi a U_\infty \sin(\alpha + \beta)$$

$$C_L = \frac{1}{V} \frac{K}{2c_1} \quad (K)$$

D. To determine the streamlines and velocity distribution along streamlines in the  $Z'$  plane:

1. Select values of  $\psi$ .

2. For values of  $r'$  calculate  $\theta'$  from

$$\sin \theta' = -\frac{1}{V} \frac{r'}{r'^2 - a^2} \left( x + \frac{K}{2\pi} \ln \frac{r'}{a} \right).$$

3. For each value of  $z' = r'e^{i\theta'}$ , the velocity at the point can be calculated from

$$u' = -V \left( 1 - \frac{a^2}{r'^2} \cos 2\theta' \right) - \frac{K}{2\pi r'} \sin \theta'$$

$$v' = V \frac{a^2}{r'^2} \sin 2\theta' + \frac{K}{2\pi r'} \cos \theta'$$

$$q' = \sqrt{u'^2 + v'^2}$$

E. Procedure for rotating the streamlines from the  $Z'$  plane to the  $Z$  plane and for transforming the streamlines from the  $Z$  plane to the  $z$  plane:

$$Z = r e^{i\theta}$$

$$Z = z' e^{i\theta'} + m e^{i\delta}$$

$$x = r' \cos(\theta' - \alpha) + m \cos \delta$$

$$y = r' \sin(\theta' - \alpha) + m \sin \delta$$

$$\xi = \left(r + \frac{C_1^2}{r}\right) \cos \theta = x \left[1 + \frac{C_1^2}{x^2 + y^2}\right]$$

$$\eta = \left(r - \frac{C_1^2}{r}\right) \sin \theta = y \left[1 - \frac{C_1^2}{x^2 + y^2}\right]$$

F. To determine the velocity distribution along a streamline in the plane: 3

$$g = u - iv = \frac{dw}{dz} = \frac{dw}{dz'} \cdot \frac{dz'}{dz} \cdot \frac{dz}{dz}$$

$$\frac{dw}{dz'} = g' = w' - iv'$$

$$\frac{dz'}{dz} = e^{i\alpha} \quad g = g' e^{i\alpha} \frac{z^2}{z^2 - C^2} = g' \left[ \frac{x^2 + y^2}{x^2 + y^2 - C^2} \right]$$

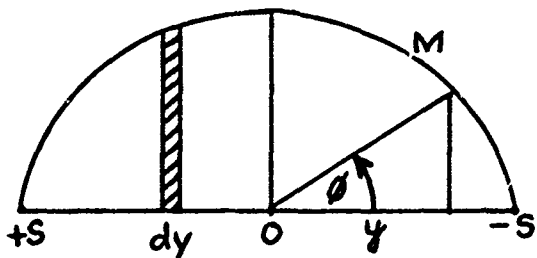
$$g = g' \frac{r^2}{[(x^2 - y^2 - C_1^2) + 4x^2 y^2]^{1/2}}$$

G. Procedure for plotting isobars around the airfoil:

First, the velocity distribution along each streamline in the <sup>3</sup> plane is plotted. Next, the streamlines around the airfoil in the <sup>3</sup> plane are plotted. Then, for chosen values of  $C_p$  the velocity is calculated;  $u = \sqrt{(1 - C_p)/2}$ . From the velocity distribution profiles, the points along the streamlines which have a velocity corresponding to the desired  $C_p$  are plotted on the streamlines around the airfoil. These points are connected to give a constant velocity line, which is also an isobar of the desired value of  $C_p$ .

APPENDIX II

DETERMINATION OF THE EFFECTIVE ASPECT RATIO AND INDUCED DRAG COEFFICIENT FROM AN ARBITRARY SPANWISE WING LOADING



Represent the spanwise loading curve by a Fourier series such as

$$M = 4SU_{\infty} \sum_{n=1}^{\infty} A_n \sin n \phi$$

$$= 4SU_{\infty} [A_1 \sin \phi + A_2 \sin 2\phi + A_3 \sin 3\phi + \dots]$$

$$y = -S \cos \phi$$

$$dy = S \sin \phi d\phi$$

$$\text{Lift} = \int_{-S}^{+S} eU_{\infty} M dy$$

$$L = \int_0^{\pi} eU_{\infty} M S \sin \phi d\phi$$

$$= \int_0^{\pi} eU_{\infty} S 4SU_{\infty} \sum_{n=1}^{\infty} A_n \sin n\phi \sin \phi d\phi$$

$$= eU_{\infty}^2 (4S^2) \sum_{n=1}^{\infty} \frac{A_n}{2} [\cos(n-1)\phi - \cos(n+1)\phi] d\phi$$

$$= eU_{\infty}^2 (4S^2) \sum_{n=1}^{\infty} \frac{A_n}{2} \left[ \frac{\sin(n-1)\phi}{n-1} - \frac{\sin(n+1)\phi}{n+1} \right]_0^{\pi}$$

$L = 0$  for all values of  $n$  except  $n = 1$

$$L = \frac{A_1}{2} \left[ \lim_{(n-1) \rightarrow 0} \frac{\sin(n-1)\phi}{n-1} \right]_{\pi}$$

$$= \frac{A_1 \pi}{2}$$

$$\therefore L = eU_{\infty}^2 (4S^2) A_1 \frac{\pi}{2} = C_L \frac{1}{2} eU_{\infty}^2 S$$

$$\therefore C_L = \pi R A_1$$

Downwash:

$$W = -\frac{1}{4\pi} \int_{-s}^{+s} \frac{(dM/dy) dy}{y-y_1} \quad \frac{dM}{d\phi} = 4SU_{\infty} \frac{d}{d\phi} \sum_{n=1}^{\infty} A_n \sin n\phi$$

$$= 4SU_{\infty} \sum_{n=1}^{\infty} n A_n \cos n\phi$$

$$W = \frac{i}{4\pi s} \int_0^{\pi} \frac{dM/d\phi d\phi}{\cos\phi - \cos\phi_1}$$

$$= \frac{4SU_{\infty}}{4\pi s} \int_0^{\pi} \frac{\sum_{n=1}^{\infty} n A_n \cos n\phi d\phi}{\cos\phi - \cos\phi_1}$$

$$= \frac{U_{\infty}}{\pi} \sum_{n=1}^{\infty} \frac{n A_n (\sin\phi_1) \pi}{\sin\phi_1}$$

via Glauert Integral.

Thus, for any value of  $\phi$ ,

$$W = U_{\infty} \frac{\sum_{n=1}^{\infty} n A_n \sin n\phi}{\sin\phi}$$

Induced Drag:

$$D_i = \int_{-s}^{+s} c W M ds = \int_0^{\pi} \frac{e U_{\infty} \sum_{n=1}^{\infty} n A_n \sin n\phi}{\sin\phi} 4SU_{\infty} \sum_{n=1}^{\infty} A_n \sin n\phi \sin\phi d\phi$$

$$= (4S^2) (e U_{\infty}^2) \int_0^{\pi} \sum_{n=1}^{\infty} n A_n \sin n\phi \sum_{n=1}^{\infty} A_n \sin n\phi d\phi$$

$$= e U_{\infty}^2 (4S^2) \int_0^{\pi} (A_1^2 \sin^2\phi + 2A_2^2 \sin 2\phi + \dots) +$$

$$(3A_1 A_2 \sin\phi \sin 2\phi + 4A_1 A_3 \sin\phi \sin 3\phi + \dots)$$

All products of different values of  $\sin\phi$  vanish when integrated between the limits of  $\phi$  and  $\pi$ .

$$\begin{aligned} \therefore D_i &= eU_\infty^2 (4S^2) \int_0^\pi \sum_{n=1}^{\infty} n A_n^2 \sin^2 n\phi d\phi \\ &= eU_\infty^2 (4S^2) \frac{\pi}{2} \sum_{n=1}^{\infty} n A_n^2 \end{aligned}$$

but  $C_{Di} = \frac{D_i}{\frac{1}{2} eU_\infty^2 S} = \pi R \sum_{n=1}^{\infty} n A_n^2$

$$= \pi R [A_1^2 + 2A_2^2 + 3A_3^2 + 4A_4^2 + \dots]$$

but we know that  $C_L = \pi R A_1$   $\therefore A_1 = \frac{C_L}{\pi R}$

$$\begin{aligned} \therefore C_{Di} &= \pi R A_1^2 \left[ 1 + 2 \left( \frac{A_2}{A_1} \right)^2 + 3 \left( \frac{A_3}{A_1} \right)^2 + 4 \left( \frac{A_4}{A_1} \right)^2 + \dots \right] \\ &= \frac{C_L^2}{\pi R} [1 + \delta] \end{aligned}$$

where  $\delta = 2 \left( \frac{A_2}{A_1} \right)^2 + 3 \left( \frac{A_3}{A_1} \right)^2 + \dots$

when  $\delta = 0$ , i.e., when  $A_2 = A_3 = A_4 = 0$ , all coefficients but  $A_1$  are zero, then  $M = 4SU_\infty A_1 \sin \phi$

$$= 4SU_\infty A_1 \sqrt{1 - (Y/S)^2}$$

which is an elliptical distribution.

**BLANK PAGE**

UNCLASSIFIED

Security Classification

DOCUMENT CONTROL DATA - R&D		
<i>(Security classification of title, body of abstract and indexing annotation must be entered when the overall report is classified)</i>		
1. ORIGINATING ACTIVITY (Corporate author) Mississippi State University Aerophysics Department State College, Mississippi		2a. REPORT SECURITY CLASSIFICATION UNCLASSIFIED
		2b. GROUP N/A
3. REPORT TITLE AN INVESTIGATION OF END PLATES TO REDUCE THE DRAG OF PLANAR WINGS		
4. DESCRIPTIVE NOTES (Type of report and inclusive dates)		
5. AUTHOR(S) (Last name, first name, initial) Roberts, Sean C.		
6. REPORT DATE January 1966	7a. TOTAL NO. OF PAGES 55	7b. NO. OF REFS 12
8a. CONTRACT OR GRANT NO. DA 44-177-AMC-892(T)	9a. ORIGINATOR'S REPORT NUMBER(S) USAAVLABS Technical Report 65-79	
b. PROJECT NO. TASK 1P121401A14203	9b. OTHER REPORT NO(S) (Any other numbers that may be assigned this report) Research Report No. 58	
10. AVAILABILITY/LIMITATION NOTICES Distribution of this document is unlimited.		
11. SUPPLEMENTARY NOTES	12. SPONSORING MILITARY ACTIVITY U. S. ARMY AVIATION MATERIEL LABORATORIES FORT EUSTIS, VIRGINIA	
13. ABSTRACT An analytical and experimental study has been performed to determine the optimum design of end plates which have minimum parasite drag and maximum effect on induced drag. Experiments were performed in a smoke tunnel and at full-scale Reynolds numbers on a modified PA-12 Super Cub aircraft. Flat end plates were found to be relatively ineffectual as a means of reducing the induced drag of aircraft, and the undesirable effect of large flat plates on the directional stability of an aircraft was an important effect to be considered. Cambered wing tip plates are worthy of further consideration, since a 15 percent decrease of induced drag with a 12 percent increase of L/D ratio was obtained from the configurations tested.		

DD FORM 1473  
1 JAN 64

UNCLASSIFIED

Security Classification

UNCLASSIFIED

Security Classification

14. KEY WORDS	LINK A		LINK B		LINK C	
	ROLE	WT	ROLE	WT	ROLE	WT

INSTRUCTIONS

1. **ORIGINATING ACTIVITY:** Enter the name and address of the contractor, subcontractor, grantee, Department of Defense activity or other organization (*corporate author*) issuing the report.

2a. **REPORT SECURITY CLASSIFICATION:** Enter the overall security classification of the report. Indicate whether "Restricted Data" is included. Marking is to be in accordance with appropriate security regulations.

2b. **GROUP:** Automatic downgrading is specified in DoD Directive 5200.10 and Armed Forces Industrial Manual. Enter the group number. Also, when applicable, show that optional markings have been used for Group 3 and Group 4 as authorized.

3. **REPORT TITLE:** Enter the complete report title in all capital letters. Titles in all cases should be unclassified. If a meaningful title cannot be selected without classification, show title classification in all capitals in parenthesis immediately following the title.

4. **DESCRIPTIVE NOTES:** If appropriate, enter the type of report, e.g., interim, progress, summary, annual, or final. Give the inclusive dates when a specific reporting period is covered.

5. **AUTHOR(S):** Enter the name(s) of author(s) as shown on or in the report. Enter last name, first name, middle initial. If military, show rank and branch of service. The name of the principal author is an absolute minimum requirement.

6. **REPORT DATE:** Enter the date of the report as day, month, year, or month, year. If more than one date appears on the report, use date of publication.

7a. **TOTAL NUMBER OF PAGES:** The total page count should follow normal pagination procedures, i.e., enter the number of pages containing information.

7b. **NUMBER OF REFERENCES:** Enter the total number of references cited in the report.

8a. **CONTRACT OR GRANT NUMBER:** If appropriate, enter the applicable number of the contract or grant under which the report was written.

8b, 8c, & 8d. **PROJECT NUMBER:** Enter the appropriate military department identification, such as project number, subproject number, system numbers, task number, etc.

9a. **ORIGINATOR'S REPORT NUMBER(S):** Enter the official report number by which the document will be identified and controlled by the originating activity. This number must be unique to this report.

9b. **OTHER REPORT NUMBER(S):** If the report has been assigned any other report numbers (*either by the originator or by the sponsor*), also enter this number(s).

10. **AVAILABILITY/LIMITATION NOTICES:** Enter any limitations on further dissemination of the report, other than those imposed by security classification, using standard statements such as:

- (1) "Qualified requesters may obtain copies of this report from DDC."
- (2) "Foreign announcement and dissemination of this report by DDC is not authorized."
- (3) "U. S. Government agencies may obtain copies of this report directly from DDC. Other qualified DDC users shall request through \_\_\_\_\_."
- (4) "U. S. military agencies may obtain copies of this report directly from DDC. Other qualified users shall request through \_\_\_\_\_."
- (5) "All distribution of this report is controlled. Qualified DDC users shall request through \_\_\_\_\_."

If the report has been furnished to the Office of Technical Services, Department of Commerce, for sale to the public, indicate this fact and enter the price, if known.

11. **SUPPLEMENTARY NOTES:** Use for additional explanatory notes.

12. **SPONSORING MILITARY ACTIVITY:** Enter the name of the departmental project office or laboratory sponsoring (*paying for*) the research and development. Include address.

13. **ABSTRACT:** Enter an abstract giving a brief and factual summary of the document indicative of the report, even though it may also appear elsewhere in the body of the technical report. If additional space is required, a continuation sheet shall be attached.

It is highly desirable that the abstract of classified reports be unclassified. Each paragraph of the abstract shall end with an indication of the military security classification of the information in the paragraph, represented as (TS), (S), (C), or (U).

There is no limitation on the length of the abstract. However, the suggested length is from 150 to 225 words.

14. **KEY WORDS:** Key words are technically meaningful terms or short phrases that characterize a report and may be used as index entries for cataloging the report. Key words must be selected so that no security classification is required. Identifiers, such as equipment model designation, trade name, military project code name, geographic location, may be used as key words but will be followed by an indication of technical context. The assignment of links, rules, and weights is optional.

UNCLASSIFIED

Security Classification